The Thesis Committee for Matthew Ronald Monette
Certifies that this is the approved version of the following Thesis:

Investigation for the Integration of Associated Produced Gas into Low Tension Gas Floods

APPROVED BY
SUPERVISING COMMITTEE:

Quoc Nguyen, Supervisor

Maša Prodanović

Investigation for the Integration of Associated Produced Gas into Low Tension Gas Floods

by

Matthew Ronald Monette

Thesis

Presented to the Faculty of the Graduate School of

The University of Texas at Austin

in Partial Fulfillment

of the Requirements

for the Degree of

Master of Science in Engineering

The University of Texas at Austin

May 2020

Dedication

To my family, friends, and peers who have helped and inspired me along the way. Your encouragement and support have been greatly appreciated.

Acknowledgements

I would like to express my sincere appreciation and gratitude to Dr. Quoc P. Nguyen for his expertise and guidance throughout the course of my learning. Without his knowledge and support I would not have been able to achieve the success I have at the University of Texas at Austin while working within his research group. I would like to thank Nhut Nguyen and Alolika Das for their direct assistance, guidance, and input throughout both successful and unsuccessful experiments. Their support and training during the early stages of my research helped develop the foundational procedural knowledge required to succeed. I would also like to thank Mr. Glen Baum and Mr. Gary Miscoe for their technical support and timely assistance during the course of my research. Finally I would like to thank Shell and the CEOR Consortium at UT for their financial and material support in completing my research.

Abstract

Investigation for the Integration of Associated Produced Gas into Low Tension Gas Floods

Matthew Ronald Monette, M.S.E

The University of Texas at Austin, 2020

Supervisor: Quoc P. Nguyen

With increased environmental restrictions, flaring may no longer remain an option for dealing with produced hydrocarbon gas in the oil field. One possible solution for responsibly handling this gas is to reinject it into the reservoir through an injection well. Gas floods have long been used for enhanced oil recovery, however they oftentimes require miscible conditions within the reservoir. If this reservoir has been depleted and no longer contains the internal pressure to achieve these miscible conditions, an enhanced oil recovery technique known as Low Tension Gas (LTG) may be a better alternative that is a promising tertiary oil recovery technology in low permeability reservoirs. This LTG process is a technique that involves either co-injection or alternating injection of gas as a mobility control agent to improve sweep efficiency, paired with an optimized surfactant formulation that is able to generate ultra-low interfacial tension (IFT) between the oil and aqueous phases. This reduced IFT allows for the previously trapped oil to become mobile and the added mobility control from the in-situ generated foam better allows for this mobile oil to exit the porous media.

An experimental investigation of typically produced hydrocarbon gas was conducted through a series of tests including phase behavior tests, dynamic foam strength

tests, and oil recovery corefloods. These tests were performed over a range of temperature, pressure, and salinity values. The impact of hydrocarbon gas as the co-injected gas was investigated and found to be not only compatible with, but ultimately beneficial to the LTG process. The use of hydrocarbon gas at elevated pressures had a notable impact on phase behavior by slightly lowering the optimum salinity, while significantly increasing the solubilization ratio. This increase in solubilization ratio corresponds to a lower IFT experienced between the oil and aqueous phases, leading to improved oil recovery. This investigation also noted that in the presence of Type I microemulsion, foams created using a hydrocarbon gas composition appeared to produce a slightly lower foam strength than that of previously used nitrogen. However, this slight decrease in foam strength was more than offset by the significant increase in solubilization ratio. Using different hydrocarbon gas compositions for the injected gas during a series of corefloods presented an increase in both the recovery rate and ultimate recovery. This suggests that repurposing produced hydrocarbon gas may not only be the environmentally responsible decision but also economically advantageous as this may allow for a decrease in surfactant costs used within a Low Tension Gas flood while still achieving the same improved oil recovery.

Table of Contents

List of Tables

List of Figures

CHAPTER 1: Introduction

1.1 Overview

Low Tension Gas (LTG) flooding is a novel chemical enhanced oil recovery technique that has been gaining increased interest in recent years as companies are continuously trying to exploit tighter conventional oil reservoirs. This Low Tension Gas process utilizes similar principles to surfactant polymer floods in which it hopes to generate both low interfacial tension between the aqueous and oil phases, while also providing improved mobility control to increase sweep efficiency and displace the newly mobilized oil. The difference between these two techniques comes from how they each try to generate this improved mobility control. Whereas polymer floods use the injected polymer to improve mobility control through increased liquid viscosity, LTG uses a co-injected gas to generate an aqueous foam which can significantly increase the apparent viscosity, thus improving the mobility control. Due to this replacement of polymer with gas for mobility control, LTG floods can be applied to more challenging reservoirs such as those with high salinity or low permeability.

Previous LTG investigations have focused primarily on floods that have utilized nitrogen gas (N_2) as the injected gas of interest. However, a reliable nitrogen gas source may not always be readily accessible. This gas availability and its associated cost may be a major challenge when considering the economic feasibility of implementing this technology at the field scale. The cost of importing or on-site generation of nitrogen gas can be significantly reduced or eliminated if produced gas from the oil field can be reprocessed and reinjected as the co-injected gas for mobility control. This injection of associated field gas would not only satisfy the gas supply need but would also responsibly satisfy environmental concerns regarding the management of produced gas and mitigate any environmental impacts. As such, this study will begin to assess the performance and economic feasibility of implanting produced field gas into the Low Tension Gas Design.

1.2 Research Motivation and Objectives

The motivation behind this research was to investigate whether the use of produced hydrocarbon gas was a viable gas option to implement into the LTG design. This feasibility could be determined if laboratory corefloods show that associated gas could perform equally, if not better than, previously used nitrogen as the co-injected gas. If successful, the use of produced field gas in the LTG design has a potential to:

1. Eliminate the need to flare produced gas in the field.
2. Eliminate the financial burden of transporting in or the on-site generation of nitrogen (N_2) gas.
3. Maintain or improve the recovery rate and ultimate recovery through favorable interactions between the hydrocarbon gas and the crude oil system.
4. Reduce overall chemical costs associated with a Low Tension Gas EOR project.

The achievement of these four objectives would improve the overall LTG project success and economic feasibility. We next describe the methodology for evaluating the above objectives.

1.3 Research Methodology and Hypothesis

The first step to determine how best to accomplish the previously mentioned research objectives is to perform a thorough literature review of previous LTG investigations to obtain pertinent knowledge as to how hydrocarbon gas my affect different aspects of the process. This preliminary review included analyzing how hydrocarbon gas could affect the two main components of the LTG process, the reduced IFT of the microemulsion phase behavior, and the improved mobility control of the in-situ generated foam. This investigation led to the understanding that typically produced field gas compositions could have a significant impact on both of these aspects, and lead to a more thorough investigation. Both of these components were decoupled from the procedure and a comprehensive characterization was performed.

A stable and successful surfactant formulation was first generated for each specific crude oil system under investigation. These surfactant formulations must be able to

maintain aqueous stability, generate ultra-low IFT between the aqueous and oil phases, and generate an adequate foam strength for the desired mobility control. These selected surfactant formulations were initially determined at atmospheric pressure before they were moved to the high pressure cell to analyze the high pressure phase behavior. The high pressure cell determined what impact different hydrocarbon gas compositions at different pressures would have on the microemulsion phase behavior, and these findings were used to better design and interpret the subsequent oil recovery corefloods. The influence of gas type on foam strength was next evaluated. This extensive study investigated a series of dynamic foam strength corefloods under a variety of conditions to determine what impact gas type had under each of these conditions. These conditions included varying salinity, pressure, presence of oil, and foam quality.

Using the information gathered during the characterization of microemulsion phase behavior and foam strength, proof of concept LTG oil recovery corefloods were performed in two different low permeability sandstone and carbonate reservoir systems. These coreflood designs utilized the newfound understanding of hydrocarbon gas impact on the LTG process to design successful oil recovery corefloods that were able to improve oil recovery rate and ultimate recovery while also utilizing a variety of techniques that would be able to reduce costs of an LTG project if implemented at the field scale.

CHAPTER 2: Literature Review of Foam and the LTG Process

2.1 Introduction to Low Tension Gas (LTG) Flooding

Low Tension Gas flooding is an EOR technique that has been proposed as a promising alternative to polymer flooding in previously deemed challenging sandstone and carbonate reservoirs such as those that are low permeability (sub 10 mD), high temperature (>100ºC) or high salinity (>150,000 ppm), or where the implementation of a negative salinity gradient may not be feasible (Srivastava et al. 2009, Das et al. 2018, 2020). The LTG process is a technique that involves the co-injection or alternating injection of gas as a mobility control agent, accompanied by an optimized surfactant formulation that is able to generate ultra-low interfacial tension between the oil and aqueous phases. The reduction of the interfacial tension between the oil and water phases allows for the mobilization of this previously immobile trapped oil, and the added mobility control from the aqueous foam improves transport and sweep efficiency.

Many previous studies have analyzed the impact and efficiency of utilizing foam as a mobility control agent. Shi and Rossen (1998) and Blaker et al. (2002) proved that surfactant alternating gas (SAG) or the gas/liquid co-injection can substantially improve mobility control and sweep efficiency, leading to higher ultimate recovery. Srivastava et al. (2009, 2010) suggested foam provided more efficient mobility control compared to polymer, finding that alkali surfactant gas (ASG) floods showed improved oil recovery and lower pressure gradients when compared to alkali surfactant polymer (ASP) floods. A study by Kamal and Marsden (1973) was one of the first studies that suggested foam was more economical than polymer when they investigated LTG floods in high permeability sandpacks. The use of the LTG process and foam as the mobility control agent becomes ever more appealing as you approach lower permeability (<100mD) sandstone and carbonate reservoirs. At these significantly lower permeabilities polymers are no longer a physically feasible or economically viable option because of the resulting plugging and shear degradation of the polymer (Martin 1986, Sorbie 1991). These low permeability

limitations of polymer are what make foam generation a more desirable mobility control agent in many tight reservoirs.

2.2 Dynamics of Aqueous Foam in Porous Media

2.2.1 Foam Induced Fluid Mobility Reduction

The aqueous foams generated within the reservoir during the co-injection of surfactant and gas in Low Tension Gas floods can be described as the dispersion of gas bubbles within a continuous liquid phase and are able to increase the effective viscosity. These gas bubbles are separated by thin liquid films known as lamellae (Schramm 1994). Within the porous reservoir flowing fluids will typically prefer to flow as a continuous phase through the larger pores or the higher permeability zones. With the co-injection and flow of both surfactant solution and gas this can create a discontinuous gas phase in the liquid. This discontinuous gas phase, or dispersion of gas bubbles within the continuous liquid media is what we refer to as foam. As these gas bubbles and liquid lamellae propagate through the pore network they experience forces resistant to flow, which in turn generates a higher apparent viscosity. This resistance to gas flow increases the gas saturation within the pore space, which in turn decreases liquid saturation. A decrease in liquid saturation initiates a decrease in liquid mobility. This increase in apparent viscosity and decrease in liquid mobility from the foam has the ability to increase sweep efficiency by improving the overall mobility control of the flowing fluid. This will help divert the flow of surfactant solution to low permeability zones of previously unswept oil.

2.2.2 Foam Generation

This in-situ foam is generated in a variety of ways, but primarily through the mechanisms known as capillary snap-off, lamella division, or lamella leave-behind. Capillary snap-off is likely the preferred mechanism for initial foam generation and is affected by the system fluid properties and pore shape geometry seen in Figure 2.1 (Kovscek and Radke 1993). Due to a decrease in the radius of curvature seen within the pore throats, elevated capillary pressure is experienced. With a reduced pressure of the gas phase and an elevated pressure of the liquid phase within the pore space, this will drive

liquid from the pore space to the pore throat increasing the liquid saturation (Ransohoff and Radke, 1988). This increased liquid saturation further develops into the previously mentioned liquid films known as lamellae.

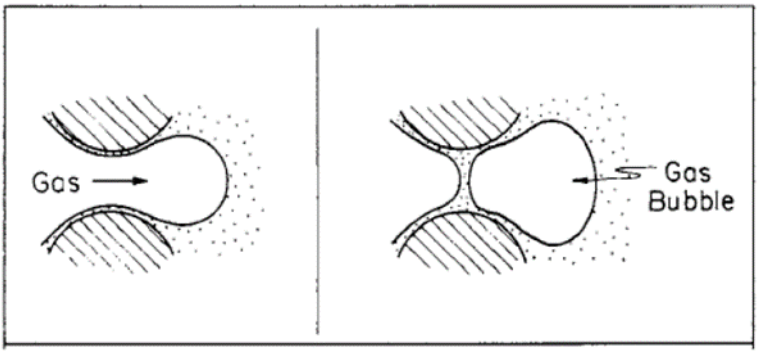

Figure 2.1 Capillary snap-off generation (Ransohoff and Radke, 1988)

While capillary snap-off may be responsible for initial foam generation, subsequent regeneration of foam is likely a resultant of lamella division (Figure 2.2) or lamella leave-behind (Figure 2.3). Lamella division requires previously formed moving lamella to encounter a branching point within the porous media were the existing lamella is split among the different available pore throats. Whereas lamella leave-behind is achieved when the gas enters a pore body previously occupied by the wetting liquid phase and lamellae are left behind in the pore throats (Ransohoff and Radke, 1988).

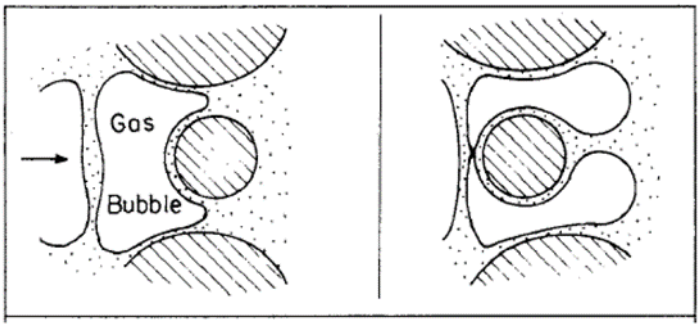

Figure 2.2 Lamella division generation (Ransohoff and Radke, 1988).

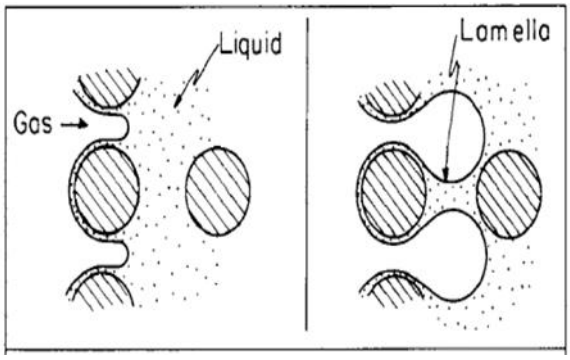

Figure 2.3 Lamella leave-behind generation (Ransohoff and Radke, 1988).

2.2.3 Foam Degradation and Destruction

Aqueous foam in and of itself is inherently unstable, and its stability is a resultant of liquid lamellae resistance to rupture. The addition of surfactant in the aqueous solution acts to improve the strength of these lamellae. Even with surfactant for improved stability, foam will still degrade and rupture through several mechanisms of drainage, disjoining pressure, and gas diffusion.

Drainage of liquid lamellae films occurs in two forms, capillary drainage and gravity drainage. The capillary drainage is a result of a pressure differential across the lamella due to the curved nature of the thin film. The lamellae have a much greater curvature near the edges as opposed to the center. This results in a higher pressure in the center of the film which will drive liquid flow towards the edges, reducing the thickness of the lamella. Once this thickness is reduced beyond a critical thickness, the liquid film will rupture (Chambers and Radke 1991). Gravity drainage as a mechanism of foam destruction is far less prominent in LTG floods, as its effect is more pronounced in thick films where liquid viscosity is a significant factor behind liquid drainage.

Disjoining pressure is a force acting along the film interface which can resist the thinning forces created by capillary drainage and will influence foam stability. A positive disjoining pressure will improve film stability while a negative disjoining pressure will act to reduce film stability. A positive disjoining pressure can be partially maintained by the electrical double layer created by the presence of surfactants adhering to and acting along the gas and liquid interface. While these surfactants act to improve foam stability, a

molecular interaction known as the van der Waals force will act to decrease this disjoining pressure.

Gas diffusion as a foam destruction mechanism is generated by the disparity in the distribution of gas bubbles in the aqueous foam. The foam within the porous media will generate gas bubbles of varying sizes. Physical properties associated with bubble size and the resulting radius of curvature will create a higher gas pressure experienced within the smaller bubbles. This pressure difference can then create a potential difference that will drive gas from the smaller bubbles towards the low pressure gas in the larger bubbles.

2.3 Gas Composition and its Impact on Characterization of the LTG Process

2.3.1 Gas Composition

The bulk of past studies on LTG floods under these similar low permeability conditions had primarily focused on nitrogen as the co-injected gas for mobility control (Srivastava et al. 2009, 2010, Das et al. 2016, 2018, 2020, Szlendak et al. 2012, 2016). The purpose of this study was to begin to determine the feasibility of using a produced gas in the oil field instead of transporting in a procured gas. Associated field gases are seen to be produced having a large variety of gas compositions. These compositions consisted primarily of hydrocarbon components with the produced hydrocarbon phase ranging from a lean gas of nearly pure methane (CH_4) to a more enriched gas consisting of roughly 85% CH_4 and 15% of heavier C_2^+ hydrocarbon gas components (Burruss and Ryder 2014).

2.3.2 Impact on Microemulsion Phase Behavior

2.3.2.1 Surfactants and Generated Microemulsion

During the LTG process surfactants are introduced into the oil reservoir in an aqueous solution in the expectation of increasing oil recovery. These surfactants are surface active agents consisting of a hydrophilic head group and a hydrophobic tail group. These surfactants will congregate along the fluid/fluid interfaces of immiscible fluids and can reduce the interfacial tension between the two fluids (oil and water). The performance and success of surfactants' ability to generate microemulsion is dependent upon a variety of

conditions, primarily the composition of the crude oil, the reservoir temperature, and the reservoir brine salinity. The specific surfactant formulation selected for each reservoir is dependent upon these factors and the quality of microemulsion that they can generate under the reservoir conditions.

Surfactants in an oil/water system have the ability to generate three different types of microemulsion, and which type of microemulsion is generated most directly correlates to reservoir electrolyte concentration otherwise referred to as salinity. These three different types of microemulsion are as follow (Green and Willhite 1998):

- Type I microemulsion consists of two distinct phases. One phase is oil solubilized micelles dispersed in the aqueous phase, and the other is an excess oil phase. This microemulsion occurs at the lower salinity range.
- Type II microemulsion also consists of two distinct phases. This includes water solubilized micelles dispersed in the oil phase, and an excess water phase. This Type II microemulsion occurs at the higher salinity range.
- Type III microemulsion consists of three distinct phases. These are an excess water phase, an excess oil phase, and a third phase existing between the two excess fluid phases consisting of both oil and water solubilized micelles. This Type III microemulsion occurs at an intermediate salinity between the Type I and Type II microemulsion.

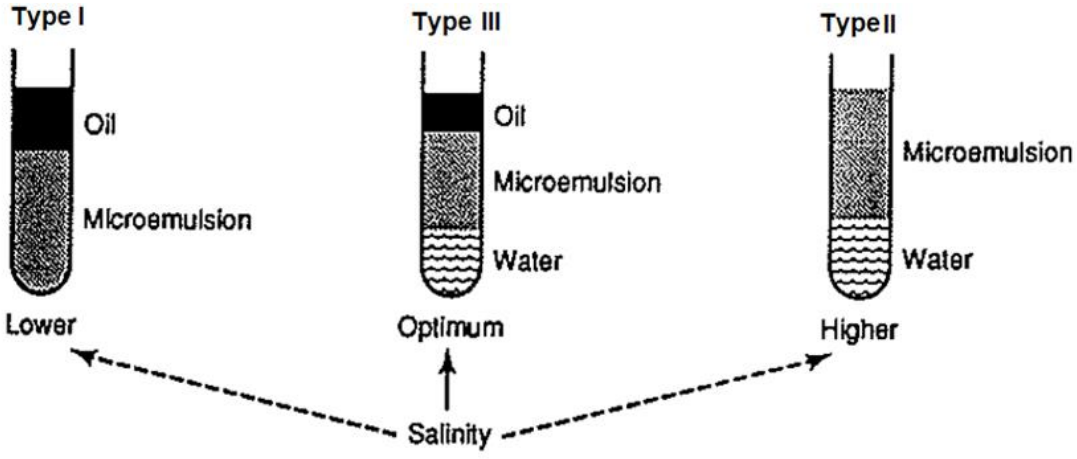

Figure 2.4 Three types of generated microemulsion (Green and Willhite, 1998).

This Type III microemulsion is most noteworthy for generating the lowest interfacial tension exhibited between the oil and aqueous phases. This reduction in IFT is maximized where the solubilization ratios of oil and water are equal. It is the generation of this Type III microemulsion that often determines the ideal surfactant formulation and salinity.

2.3.2.2 Impact of Hydrocarbon Gas at Elevated Pressure

There has been ample research on the effect of gas type on microemulsion phase behavior. Altering the gas composition at elevated pressures during phase behavior can have a variety of effects on surfactant performance and the subsequent solubilization of oil and water. As the LTG process is predominantly performed as a tertiary recovery technique, the crude oil within the system is likely reduced towards characteristics most similar to a dead oil. Conducting these LTG floods with a hydrocarbon gas at elevated reservoir pressures, one would expect a noticeable amount of this gas to dissolve back into the oil phase, even without completely miscible conditions. This dissolution of gas into the oil phase would shift oil phase characteristic back towards those more representative of live oil.

Recent microemulsion phase behavior studies by Jang et al (2014) have shown that there can be a significant difference in phase behavior properties between dead and live oils. Experimental studies (Puerto and Reed 1983; Roshanfekr et al. 2009; Southwick et al. 2012) concluded that methane causes a decrease in optimum salinity when added to dead crude oil. Phase behavior studies by Sagi et al. (2013) and Lu et al. (2013) also observed that the addition of methane and ethane to dead oil resulted in a decrease in Type III optimum salinity. In addition to decreasing the optimum salinity the dissolution of hydrocarbon gas back into the oil phase can increase the solubilization ratios, thus further reducing the interfacial tension between oil and water. Water and oil solubilization ratios increased with the addition of solution gas in studies by Jang et al. (2014). While the majority of studies showed the decreasing trend in optimum salinity, there were however some contradictory studies that showed an increase in optimum salinity for a live oil (Cottin et al. 2012). This suggests that these trends are not certain, and must be examined for each

crude oil and surfactant system. In addition to simply the effect of hydrocarbon gas, other researchers also found that an increase in pressure decreased the optimum salinity in crude oils (Kim et al. 1985, 1988; Austad et al. 1990, 1996). An attempt to quantify this decrease in optimum salinity with an increase in pressure was performed throughout a series of studies by Bourrel and Schechter (1988, 2010). Increasing system pressure causes the molecules to move closer together, increasing both hydrophilic and hydrophobic interactions. In systems composed primarily of oil and water the hydrocarbons are generally significantly more compressible. This increases the hydrocarbon cohesive energy and in turn lowers the optimum salinity and increases the solubilization ratio. It is seen from this extensive review of previous research that the addition of solution gas at elevated pressures may have a remarkable impact on shifting the optimum salinity and solubilization ratios.

2.3.3 Impact of Hydrocarbon Gas on Foam Strength in Porous Media

As with phase behavior, foam strength is expected to be significantly impacted by both the injected gas composition and the reservoir pressure.

2.3.3.1 Gas Composition

Some previous researchers such as Zeng et al. (2016), Neethling et al. (2005), and Saint-Jalmes (2006) have noted that gas composition has an impact on foam stability. There is existing theory that suggests foam strength is directly influenced by gas-phase properties such as its solubility into the aqueous phase and the foam film relative permeability. Two processes responsible for the alteration in foam stability involve the diffusion of gas through the liquid lamellae and the collapse of the liquid lamellae with the subsequent coalescence of the contiguous gas bubbles. In this way the gas composition affects overall foam strength as the solubility constant of each gas differs and as the solubility constant changes lamellae drainage rates scales along with the solubility constant (Farajzadeh 2014). With hydrocarbon gases having a larger permeability coefficient it may be expected that these generated foam films would have a higher drainage rate and thus a reduction in the lamella stability.

The gas composition can also impact the degree to which oil spreading across the foam interface occurs. As seen with the impact of gas composition on microemulsion, the dissolution of lighter hydrocarbons into the oil phase can decrease the oil viscosity and density. This creates oil swelling which can be detrimental to foam strength through alterations to the entry, spreading, and bridging coefficients of the gas (Osei-Bonsu et al. 2015). As the density and viscosity of an oil decrease it can be expected to experience more dispersion of these oil swollen micelles on the foam film, reducing its stability.

2.3.3.2 Gas Pressure

There have been previous studies performed on the effect of pressure on foam strength, with the overwhelming consensus being that increased pressure in the presence of sufficient surfactant acts to stabilize foam (Maini 1986, Holt et al. 1996). This observation can be explained by the reduction of the surface tension of surfactant solutions at high pressures due partly to the reduced density difference between the gas and liquid phases. An increase in pressure also presents a negative contribution to the disjoining pressure because of a reduction in the van der Waals effect, leading to a more stable foam (Holt et al. 1996).

2.4 Chapter summary

Previous Low Tension Gas studies had been conducted primarily with the use of nitrogen gas as the mobility control agent. In an attempt to make the implementation of an LTG flood more economical and applicable at the field scale produced hydrocarbon gas as an alternative to nitrogen was investigated. While there are previous studies that have analyzed the impact of solution gas on the individual components of an LTG flood, there are very few studies that have looked at the overall effect on an oil recovery coreflood. Therein of itself presents the need to further investigate the overall performance of different hydrocarbon gas compositions on the success of an LTG flood. The knowledge procured from previous studies analyzing the impact of hydrocarbon gas has been critical in the design and implementation of our conducted experimental plan.

CHAPTER 3: Feasibility of Produced Gas Implementation into the LTG Design under Moderate Conditions

3.1 Introduction

The objective of this chapter is to begin to conduct a thorough characterization of the impact produced gas can have on the major components of an LTG flood. This characterization was conducted under moderate reservoir conditions and these conditions were varied to further understand any inherent effects. The first step for this investigation required the development of a successful surfactant formulation for the desired crude oil that would be used. Next the different components of the LTG design were decoupled from the overall design to better understand the gas compositions direct effect. With a comprehensive characterization of these effects, a series of proof of concept corefloods were conducted to display the added benefits that could be expected with the transition from nitrogen gas to a variety of different produced field gases.

3.2 Experimental Materials

3.2.1 Synthetic Brine

The formation brine salinity for this study was set at 95,000 ppm for the total dissolved solids (TDS) consisting of 85,000 ppm NaCl and 10,000 ppm Na_2CO_3. This addition of sodium carbonate (Na_2CO_3) is a commonly used alkali to prevent carbonate precipitation and reduce surfactant absorption onto the rock surface (Hirasaki et al, 2008). This brine formulation was also used as the synthetic brine for the waterflood and slug injection during the coreflood experiments. The brine used for the lower salinity drive injection had a TDS of 80,000 ppm, with 70,000 ppm NaCl and 10,000 ppm Na_2CO_3. This brine was prepared by dissolving the specific weight percent of solid into de-ionized water to prepare the brine at the desired salinity.

3.2.2 Chemical Surfactant Formulation

The surfactant slug formulation used for these coreflood experiments was designed to achieve optimum salinity near that of the formation and waterflood brine salinities. This formulation involved the combination of a carboxylate which generates significant oil/water microemulsion for significantly reducing the interfacial tension, an internal olefin sulfonate (IOS) which has been shown to demonstrate favorable foaming abilities at low concentrations, and a TGBE co-solvent which was added to improve equilibration time and aqueous stability. The optimum Type III salinity at atmospheric pressure and reservoir temperature is shown in Figure 3.1. This Type III microemulsion environment ranged between 85,000 and 115,000 ppm.

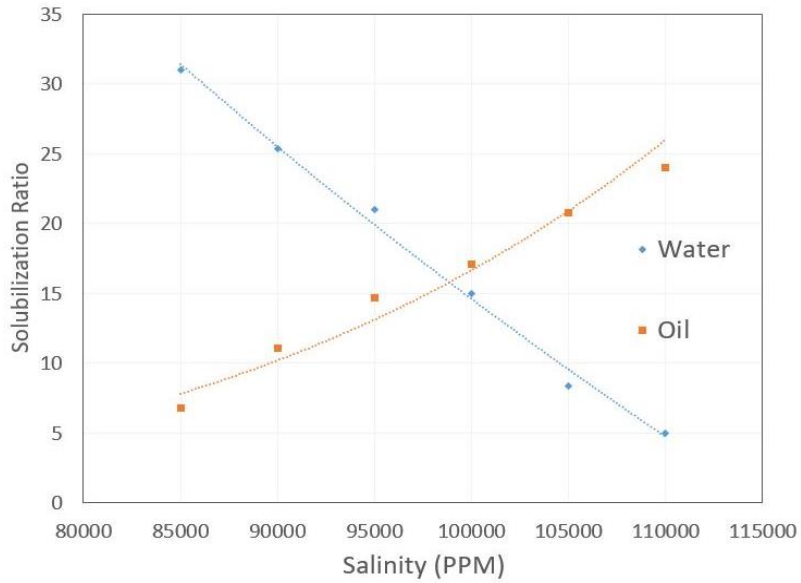

Figure 3.1. Water and oil solubilization ratios at ambient pressure and 52ºC.

3.2.3 Crude Oil

The crude oil used for this investigation had a density of 0.85 g/cm^3 and a measured viscosity 7.04 cP at 52 ºC. Before any experimental procedures were performed, this given crude was filtered with 1.2-micron filter paper to remove any suspended solids and fine particles.

3.2.4 Injection Gas

The main objective of this investigation is to characterize the varying effects that the injected gas can have on the LTG process. Three different gas compositions were used throughout the course of this study. These gases consisted of pure nitrogen (N_2) for our reference case, and two different hydrocarbon gases. The two hydrocarbon gases under investigation were selected to simplify and model both ends of a typical produced gas composition spectrum observed in the field, a lean produced gas modeled as methane (CH_4) with a 99% purity, and a more enriched produced gas composition consisting of 85% methane balanced by 15% (±0.5%) ethane (C_2H_6) by mole fraction.

3.2.5 Cores

Five Carbon Tan Sandstone cores were used throughout the duration of this investigation. All cores were cut in the same direction from the same sample block. These were cut parallel to the bedding plane with the dimensions 1.5 inches x 12 inches. This sample block was independently determined by the supplier to have a gas permeability of 42 mD and porosity of 12.2 - 17.7%. These cores were dry aged at 120º C for at least 10 days before use.

3.3 Experimental Procedures

3.3.1 High Pressure Microemulsion Phase Behavior

The first step in characterization of this research was to investigate the effect that gas composition at elevated reservoir pressures would have on the microemulsion phase behavior of this particular surfactant and crude oil system. A series of high pressure phase behaviors were conducted within five Separex (SC350-L P-max 350 Bar, T-max 150º C) high pressure cells. Each Separex cell was initially filled with 6.0 ml of the surfactant slug solution at the desired salinity within the phase behavior range of interest. Next, 2.0 ml of crude oil was added into the cell before being sealed. Once sealed, the desired gas composition was pumped into the high pressure cell through a valve to the desired reservoir pressure. These cells were then shaken twice daily for the first three days, then allowed to

rest until an equilibrium state was observed. The range of salinity scan for this high pressure phase behavior was determined by conducting the initial phase behavior tests at ambient pressure and reservoir temperature to first determine the Type III microemulsion window. The high pressure test was then conducted on the selected salinities within this Type III microemulsion window to determine how the optimum salinity would shift, these high pressure cells and the range of salinities tested can be seen in Figure 3.1 and Figure 3.2 in the high pressure phase behavior discussion.

3.3.2 Live Oil Swelling

In addition to determining the phase behavior at the elevated pressures, it was also noted that differing degrees of oil swelling would be achieved as the initially dead oil came in contact with the hydrocarbon gases. While these conditions were still below the miscibility pressure it was expected that some amount of C_1 or C_2 would still dissolve into the oil phase. To determine how much oil swelling could be achieved in this system an experiment was conducted in the same set of high pressure cells that were used for the phase behavior. These cells were first filled with the desired amount of crude oil and then pressurized with the desired gas composition and pressure. These cells were then shaken twice daily for the first three days to ensure mixing of the hydrocarbon gas with the oil. The volume increase of the oil phase was then recorded and the percentage increase can be seen below.

Table 3.1. Live Oil Swelling Volume Increase Due to Dissolution of Gas

Gas Composition	Pressure (psi)	Volume (%)
(CH_4)	900	4.90
	1500	8.66
(CH_4/C_2H_6)	900	9.21
	1200	13.80
	1500	17.00

3.3.3 Dynamic Foam Strength

A series of dynamic foam strength tests were conducted to determine the impact of gas composition, pressure, and salinity on the resulting foam strength. The foam strength

tests were performed using the same outcrop cores which were to be used in the following oil recovery coreflood experiments. These foam tests were done using the same coreflood set up and a similar injection procedure as would be conducted during the oil recovery corefloods in an effort to generate the most representative data set. All tests were conducted within the same core in order to assure that consistent conclusions could be formed between the different foam floods.

This sandstone core was initially saturated with formation brine to determine core properties, resulting in a core porosity of 17% and a relative permeability to brine of 35.4 mD. After initial properties of the core were determined, the first dynamic foam test was begun. These foaming tests attempted to characterize three different parameters that could be altered during the LTG flood. The first and most paramount of these was the gas composition that was injected. As the alteration of gas composition was the focus of this investigation these impacts were important to understand and quantify. The other two parameters that were changed were the pressure to determine if the impact of gas composition correlated to pressure changes, and salinity since the following proof of concept corefloods were to be implemented with a negative salinity gradient. All foaming tests were conducted as follows: the brine-saturated core was vacuumed for 8 hours before being injected with 2 pore volumes (PV) of the desired surfactant solution. Once the core was saturated with the desired surfactant solution, the co-injection of surfactant solution and gas composition began. This co-injection continued until a steady state pressure drop was observed across the core. The dynamic foam test for that particular surfactant solution and gas composition was then terminated after this pressure drop remained at steady state for longer than 0.5 injected liquid PV. After termination, the core was returned to previous coreflood conditions. This was achieved by vacuuming the core for 8 hours, injecting 2 PV of formation brine, vacuuming the core for another 8 hours, and saturating with 2 PV of the new desired surfactant solution.

The injected aqueous solution consisted of the slug solution at the desired salinity of interest. For the last several foam strength tests a Type I microemulsion was used to investigate its impact on foam strength. These dynamic foam strength tests were conducted

by first generating the Type I microemulsion at the desired salinity and then using this equilibrated microemulsion as the co-injected surfactant solution with each of the gases being investigated. The microemulsion salinities of 80,000 ppm and 90,000 ppm were chosen as the salinities of investigation as these most closely represented the microemulsion that would be found within the system of the planned oil recovery corefloods using the traditional negative salinity gradient. The dynamic foaming test results were done under a variety of conditions to further classify any deviations in foam strength seen between the different injected gases. These different parameters can be seen below in Table 3.2.

Table 3.2: Parameters of dynamic foam strength tests

Salinity (ppm)	Pressure (psi)	Gas Composition	Type I ME	Objective
90,000	**1500**	**N_2**	**No**	**Foam Strength Comparison**
90,000	**1500**	**CH_4**	**No**	**Foam Strength Comparison**
80,000	**1500**	**N_2**	**No**	**Salinity effect absent oil**
80,000	**1500**	**CH_4**	**No**	**Salinity effect absent oil**
80,000	**900**	**N_2**	**No**	**Pressure effect**
80,000	**900**	**CH_4**	**No**	**Pressure effect**
80,000	**900**	**(85%) CH_4/ (15%) C_2H_6**	**No**	**Pressure effect**
80,000	**900**	**N_2**	**Yes**	**Effect of Type I ME**
80,000	**900**	**CH_4**	**Yes**	**Effect of Type I ME**
90,000	**900**	**N_2**	**Yes**	**Salinity effect, Type I ME**
90,000	**900**	**CH_4**	**Yes**	**Salinity effect, Type I ME**

3.3.4 Oil Recovery Coreflood

All coreflood experiments were conducted using sandstone cores with the dimensions of 1.5 inches diameter and 12 inches length. These cores all had a permeability in the range of 25-35 mD. Each of the specified gases used was co-injection during both slug and drive injection at a 50% foam quality (50% liquid and 50% gas by volume). Each

core was oven-aged for 2 weeks to ensure that it had a zero initial water saturation. A schematic of coreflood apparatus is shown below in Figure 3.2 and the procedure was conducted as follows: the core was sealed within heat shrink tubing and inserted into the core holder. This core holder was then sealed by applying and tightening the top and bottom caps. Two holes were drilled into the core at 3 inches from the top and bottom, where the pressure taps (seen in Figure 3.2) would be inserted to monitor pressure drop during the duration of the flood. All pressure transducer and injection lines were connected to the core holder and the set up was leak tested for 24 hours. After satisfying the leak test, the core and system were vacuumed from top and bottom to remove all air from the system. Upon the completion of vacuuming, fluid injection was performed. Fluid injection during all phases of the coreflood were performed from bottom to top. The injected liquids were stored in piston accumulators and liquid injection rate and pressure was controlled by a Quizix QX6000SS pump. Injected gas rate was controlled by a Bronkhorst Mass Flow Controller, and constant gas pressure was controlled through the use of a back pressure regulator. Fluid injection began with brine saturation, in which the core porosity and permeability were determined. Following brine injection, the core was vacuumed from top and bottom for 8 hours to return system to connate water saturation. Crude oil was then injected and oil phase relative permeability was determined. This crude oil injection was continued until 100% oil cut was observed at the effluent. Initial oil saturation through mass balance was determined. Waterflood was next conducted and continued until 100% water cut was observed at the effluent. Chemical injection was then started with the co-injection of the optimized surfactant solution and desired gas at a 50% foam strength. This slug was switched to a drive injection following 0.5 liquid PV of injected slug, and gas injection was unaltered. Drive injection continued until 0% oil cut was observed at the effluent. These Experimental properties and injection parameters are summarized in the following Table 3.3 and Table 3.4. Experimental properties such as oil recovery, oil cut, and pressure drop were measured. Interpretations can be seen in discussion section.

Table 3.3: Properties of coreflood experiments	
Rock type	Sandstone
Length	12 in.
Diameter	1.5 in.
Temperature	52 ^{0}C
Back pressure	Varied, (900 PSI or 1500 PSI)
Water flood injection rate	2 ft./day
Slug/drive injection rate	2 ft./day (1 ft./day liquid and 1ft/day gas)
Gas type	Varied, N_2, CH_4, Mixture (85%CH_4 / 15% C_2H_6)
Water flood salinity	95,000 ppm
Slug size and salinity	95,000 ppm (0.5 wt.% 0.5 PV liquid)
Drive size and salinity	80,000 ppm (0.2 wt. % 1.5 PV liquid)

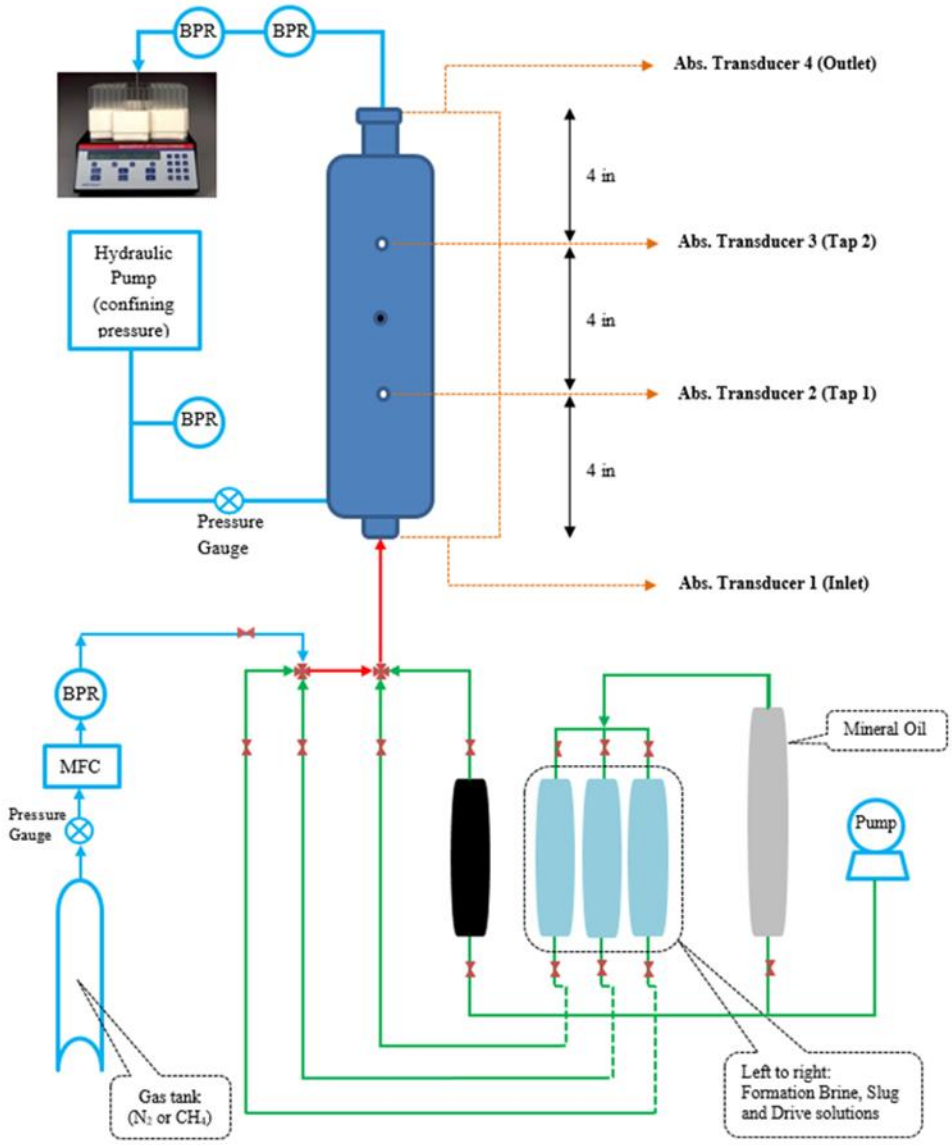

Figure 3.2 Schematic of coreflood apparatus used for dynamic foam stability and all subsequent oil recovery corefloods. BPR stands for back pressure regulator, and MFC for mass flow controller.

Table 3.4 Individual Core Properties for LTG Corefloods

Flood No.	Porosity (%)	Permeability (mD)	Reservoir Pressure (psi)	Injected gas type	Objective
1	15.2	25.4	900	N_2	Reference flood
2	15.6	27.7	900	CH_4	Effect of Methane
3	16.4	34.8	1500	CH_4	Effect of Methane at high pressure
4	16.1	28.2	900	CH_4/C_2H_6	Effect of CH4/C2H6

3.4 Experimental Results and Discussion

3.4.1 Effect of Gas Composition on Microemulsion Phase Behavior

The first effect characterized was the impact of injected gas composition on the microemulsion phase behavior, and these phase behavior results can be seen below in Figure 3.3 for the effect of methane on phase behavior at 900, 1200 and 1500 psi, and Figure 3.4 for the effect of the hydrocarbon gas mixture at 900, 1200, and 1500 psi. Throughout the salinity range of interest for the high pressure methane phase behavior in Figure 3.3 it is observed that while the pressure increases from 900 psi to 1500 psi there is only a slight shift in the Type III range as only the last cell (105,000 ppm) begins to shift into the Type II range, however there is a noticeable increase in the solubilization ratio as the middle phase observed in each cell can be seen to increase in volume as the pressure is continuously increased. These are trends that have also been seen in many previous high pressure phase behavior studies (Jang et al 2014; Roshanfekr 2009). This observation also holds true for the high pressure phase behavior seen in Figure 3.4. While the volume oil and water solubilized into the Type III microemulsion is seen to increase more significantly for the gas mixture the shift in optimum salinity is also observed to be more severe, as at 1500 psi the last two cell (100,000 ppm and 105,000 ppm) have shifted from the Type III range into the Type II range.

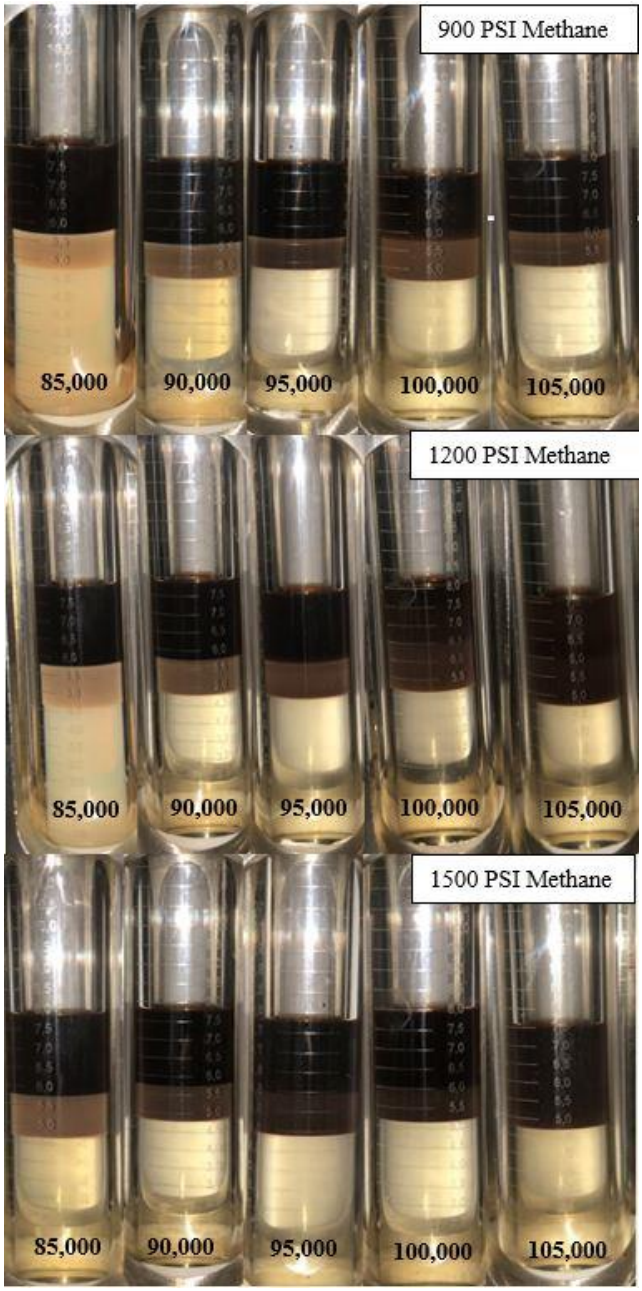

Figure 3.3 High pressure microemulsion phase behaviors with methane. Type III microemulsion is the middle phase between excess oil (darkest top phase) and water (clear bottom phase).

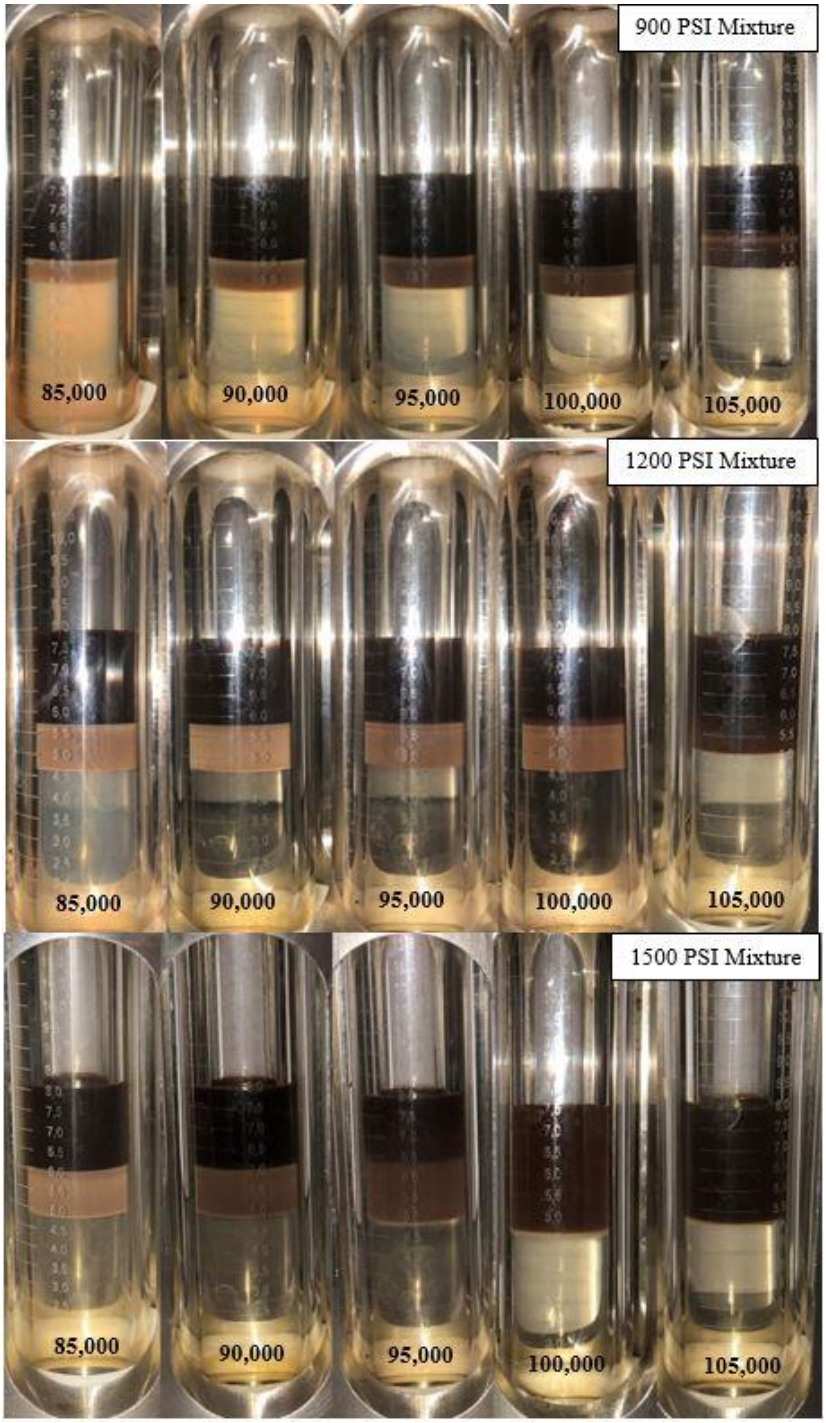

Figure 3.4 High pressure microemulsion phase behaviors with methane/ethane mixture. Type III microemulsion is the middle phase between excess oil (darkest top phase) and water (clear bottom phase).

These respective solubilization ratios for oil and water along with optimum salinity can be seen in Figure 3.5 for the pure methane, and Figure 3.6 for the methane/ethane gas mixture. From the methane graph of solubilization ratios (Figure 3.5) it is observed that the optimum salinity has only a slight decrease (~ 2,000 ppm), while the solubilization ratios increase substantially. This optimum salinity solubilization ratio increased from approximately 16 at atmospheric pressure conditions to over 20 at a system pressure of 1500 psi methane. This increased microemulsion leads to an even greater decrease in the IFT between the aqueous and oil phases.

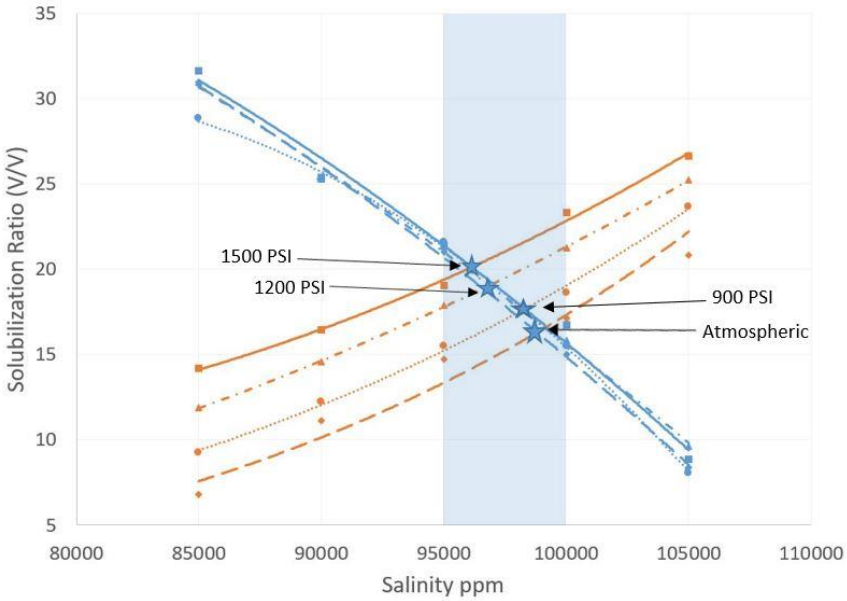

Figure 3.5 Solubilization ratios of oil and water in microemulsion as a function of methane pressure.

While the high pressure phase behavior tests using methane displayed only a slight decrease in optimum salinity, the same was not observed in the presence of the methane/ethane mixture. Figure 3.6 displays this same trend of increasing solubilization ratios with increasing pressure, however the optimum salinity decreases dramatically (~ 6000 ppm) at the higher pressures for this specific crude oil system. At 900 psi, both gas compositions had an optimum salinity similar to that observed at ambient pressure. The main difference between the gas types appeared to be an increase from a solubilization ratio at optimum salinity around 17 for the pure methane to a ratio of 18 for the

methane/ethane mixture. As the pressure was increased to 1500 psi, the solubilization ratio with pure methane increased to 20, while the enriched composition increased the solubilization ratio to over 22. This pressure effect on phase behavior can be partially explained by the molecular interactions of the surfactant. Increasing system pressures causes the molecules to move closer together which increases the hydrophilic and lipophilic interactions of the surfactant (Bourrell and Schechter 1988). In oil/water systems the hydrocarbon component is often more compressible than the aqueous phase. This will increase the hydrocarbon cohesive energy compared to that at the atmospheric state generating a stronger interaction of the surfactant at the oil water interface (Bourrel & Schechter 1988; Bourrel & Schechter 2010). This effect can likely explain the high pressure phase behavior trends of an increased solubilization ratio and a decrease in optimum salinity. The observed microemulsion phase behaviors indicate that it is possible to increase the solubilization ratio considerably by increasing either gas pressure or gas enrichment without the need for altering surfactant formulation.

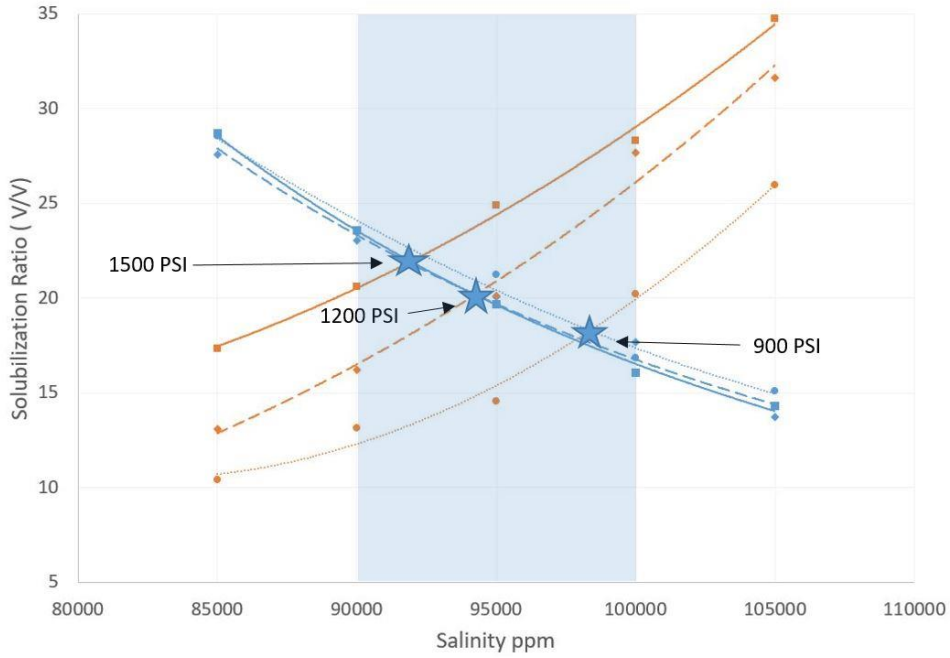

Figure 3.6 High pressure phase behaviors displaying the effect of methane/ethane mixture on solubilization ratio and optimum salinity.

Each of these phase behavior tests of the differing gas composition were repeated three times at each pressure, and a table showing the average and difference between tests is seen in Table 3.5. This low deviation supports the accuracy behind these solubilization curves, as the deviation seen between each trial using the same parameters has a smaller deviation than that observed between phase behaviors of the differing parameters. This provides confidence into the results and the reproducibility of these phase behavior experiments.

Table 3.5 Reproducibility of oil and water solubilization ratios at different pressures

Methane Average Solubilization Ratio						
Salinity	**900 psi**		**1200 psi**		**1500 psi**	
	Water (±)	**Oil (±)**	**Water (±)**	**Oil (±)**	**Water (±)**	**Oil (±)**
85,000	28.8 (2.1)	9.3 (0.5)	31.0 (1.6)	11.9 (2.3)	31.6 (0.5)	14.2 (1.1)
90,000	25.2 (1.9)	12.2 (0.8)	27.7 (1.4)	14.6 (1.9)	25.4 (1.1)	16.4 (1.2)
95,000	21.6 (0.8)	15.5 (0.5)	21.2 (0.5)	17.9 (1.1)	21.4 (0.6)	19.0 (0.6)
100,000	15.5 (1.4)	18.6 (1.2)	15.8 (0.4)	21.2 (0.9)	16.8 (0.4)	23.3 (1.3)
105,000	8.0 (1.5)	23.6 (0.4)	9.6 (1.8)	25.2 (0.6)	8.8 (0.5)	26.6 (1.1)
Methane/Ethane Average Solubilization Ratio						
Salinity	**900 psi**		**1200 psi**		**1500 psi**	
	Water (±)	**Oil (±)**	**Water (±)**	**Oil (±)**	**Water (±)**	**Oil (±)**
85,000	28.6 (0.4)	10.4 (0.7)	27.6 (0.7)	13.1 (1.5)	28.7 (0.4)	17.3 (1.5)
90,000	23.5 (0.8)	13.1 (0.7)	23.0 (0.5)	16.2 (2.0)	23.6 (1.2)	20.6 (2.1)
95,000	21.3 (1.1)	14.6 (1.3)	20.1 (1.4)	20.1 (1.8)	19.7 (0.5)	24.9 (1.6)
100,000	16.8 (0.9)	20.2 (1.7)	17.7 (1.2)	27.7 (1.7)	16.1 (1.3)	28.3 (2.3)
105,000	15.2 (1.2)	26.0 (1.5)	13.7 (0.4)	31.6 (1.6)	14.3 (0.7)	34.7 (1.9)

3.4.2 Effect of Gas Composition, Pressure, and Salinity on Foam Apparent Viscosity

The next substantial impact that injected gas composition may have on a Low-Tension Gas flood is the alteration of the foam strength or stability. This foam strength directly influences the sweep efficiency through improved mobility control provided from the in-situ generated foam during the flood. This stability was investigated for each gas, both with and without the presence of Type I microemulsion in the co-injected liquid phase. All dynamic foaming tests were conducted inside the same sandstone outcrop core which was cut from the same block as those used for the subsequent oil recovery corefloods. To better compare these results with the later oil recovery floods and previously reviewed

studies these foam strengths were recorded as their apparent viscosity at these steady state conditions. The results from the series of investigation floods performed can be seen below in Figure 3.7. The first parameter investigated was the effect of pressure and whether that generated any significant difference in foam stability between nitrogen and methane gas at the varying pressures and drive salinities in the absence of Type I microemulsion.

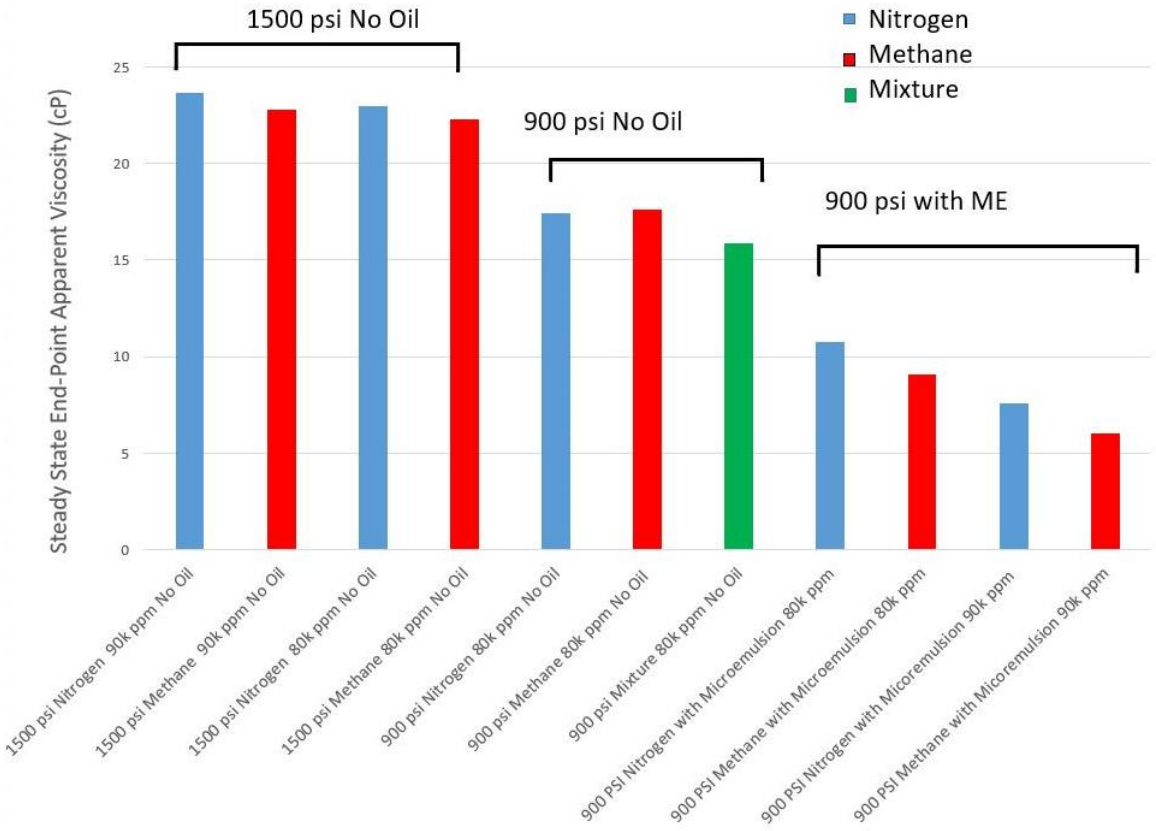

Figure 3.7 Steady-state apparent viscosity of foam under various conditions.

Looking first at the effect of gas composition at a constant salinity and pressure there appears to be minimal observable difference between the apparent viscosity achieved between the two injected gases at the 1500 psi and 90,000 ppm condition. The nitrogen gas generated only a slightly higher apparent viscosity (23.6 cp) as compared to the methane gas (22.8 cp), as seen in Figure 3.7. In addition, comparing the apparent viscosity observed between these two injected gases at the same 1500 psi pressure but at a lower aqueous salinity reveals that there is no significant effect of salinity on quasi-steady state foam

strength. This observation agrees with a previous study by Jong et al. 2016, which concluded that salinity does not have any impact on the foaming performance of the surfactants used in this work as long as the surfactant concentration is below the aqueous stability limit.

With no substantial effect of salinity on the oil free foam strength, the effect of pressure on foam strength was further investigated. System pressure was then reduced to 900 psi and comparisons were made between the steady state apparent viscosities achieved between all three of the injected gases at the lower pressure. Again, both nitrogen and methane gases achieve nearly the same steady state apparent viscosity at 900 psi pressure, while the methane/ethane mixture produced a smaller calculated apparent viscosity, suggesting a less stable foam. Comparing the effect of system pressure back to the 1500 psi system revealed a significant decrease in apparent viscosity. At 1500 psi, both nitrogen and methane generated strong foam with the apparent viscosity near 23 cp compared to less than 18 cp for the quasi-steady state foam flow at 900 psi. This suggests that a weaker foam is generated at lower pressures. This trend was also observed in Holt et al. 1996, when gas is co-injected with a liquid phase containing excess surfactant you are able to generate a stronger foam at higher pressures. This has been attributed to the reduced surface tension because of both the reduced density difference between the gas and liquid phase, but also because of increased adsorption of gas and surfactant along the liquid-gas interface.

Following the dynamic foam strength tests in the absence of oil, the impact of oil in microemulsion within the co-injected aqueous phase was investigated to determine what impact on foam strength may be generated between the investigated methane and nitrogen gases. These dynamic foam strength tests involved the pre-generated Type I microemulsion as previously described. The effects of Type I microemulsion on foam strength are shown above in Figure 3.7**.** Analysing the apparent viscosity of foam generated within the core in the presence of Type I microemulsion it is quite aparent that the presence of microemulsion has a substantial effect on foam strength. The 900 psi no oil apparent viscosity for the different gases ranged from 16 to 17.5 cp, while the highest apparent viscosity seen using

the Type I microemulsion was 10.7 cp. This immediately signals the impact that the presence of oil can have on foam stability, which has been seen in previous studies (Jong 2018). For the planned oil recovery corefloods our in-situ salinity would range from a waterflood and slug salinity of 95,000 ppm to our drive salinity of 80,000 ppm due to the desired negative salinity gradient. As the injected microemulsion salinity increased from the 80,000 ppm to 90,000 ppm the generated foams apparent viscosity is seen to decrease substantially at the higher salinity. This effect was quantified by the work conducted by Jong (2018). As the aqeuos salinity approaches that of optimum, larger amounts of oil and water are being solubilized into the Type III microemulsion phase, leaving less free surfactant within the Type I phase to act as a foaming agent along the lamella interface. In addtion, the oil swollen micelles in the Type I phase become larger as they approach optimum salinity. This increase in generated apparent viscosity at lower salinties is the reason a negative salinity injection scheme has traditionally been used in chemical EOR designs.

Comparing between the different gases absent any microemulsion the variations appeared relativly small, however with the presence of microemulsion the disparity between the different gas types becomes much more prevelant. With the presence of the microemulsion the hydrocarbon gas generated a weaker foam as seen through the reduced steady-state apparent viscosity. Osei-Bonsu et al. (2015) explained how it could be expected to observe more dispersion of oil droplets in foam films as the viscosity and the density of the oil are reduced. This reduction of oil density and viscosity is a characteristic that can be expected with the possible oil swelling at the elevated pressures and may partially explain the decrease in apparent viscosity. An addition to the reduction of oil viscosity, methane gas has a lower IFT with the crude oil when compared to nitrogen, it allows for the oil to more easily spread alongthe interface between the phases, decreasing the foam stability. This spreading of the oil along the interface between the phases can predominantly explain the differences observed between the injected gases in the presence of Type I microemulsion. A further reason associating the decrease in foam strength with the use of the hydrocarbon gas relates back to the results from the high pressure phase

behavior tests. From the solubilization curves we saw the slight reduction of optimum salinity for the hydrocarbon gases. This would place the injected microemulsion salinities closer to the optimum salinity resulting in an increase in oil dissolved into the middle microemulsion phase, this would subsequently lead to less free surfactant available in the excess aqueous phase, thus hindering the foaming performance.

3.4.3 Oil Recovery by Low Tension Gas Floods

Following the characterization of the impact of injected gas composition on the phase behavior and foam stabilty of this reservior system, proof of concept oil recovery corefloods were performed. The ultimate recovery and initial oil saturations for the four conducted corefloods are summarized below in Table 3.6**.** This table presents the initial oil saturation (S_{oi}) after primary drainage, the residual oil saturations after water flood (S_{orw}), and the oil recovery by LTG flooding from coreflood experiments. All these corefloods show similar (S_{oi}) and (S_{orw}) values, along with similar porosities and permeability's which were shown prior.

Table 3.6 Coreflood recovery results.

Coreflood	S_{oi} (%)	S_{orw} (%)	Oil Recovery* (%)	Objective
900 psi N_2	61	35	76	Reference flood
900 psi CH_4	66	31	79	Effect of methane (CH_4)
900 psi CH_4/CH_6	62	34	84	Effect of CH_4/C_2H_6 mixture
1500 psi CH_4	64	32	86	Effect of elevated pressure

* percent of residual oil after waterflood

3.4.3.1 Nitrogen Reference Coreflood 900 psi

The first coreflood performed involved nitrogen as the co-injected gas. Previous papers have found that, with nitrogen, optimum injection parameters can include a liquid slug size of 0.5 PV (pore volumes) near the Type III optimum salinity and injecting at a 50% foam quality (Srivastava and Nguyen 2010; Szlendak 2012; Szlendak et al 2016). This slug was injected with the previously stated parameters of 0.5 wt. % surfactant

followed by a 0.2 wt. % surfactant foaming drive solution. These conditions were kept constant for all four of the oil recovery corefloods. Implementing these parameters for the first coreflood, we achieved the oil recovery and pressure drop data displayed in Figure 3.8 and 3.9.

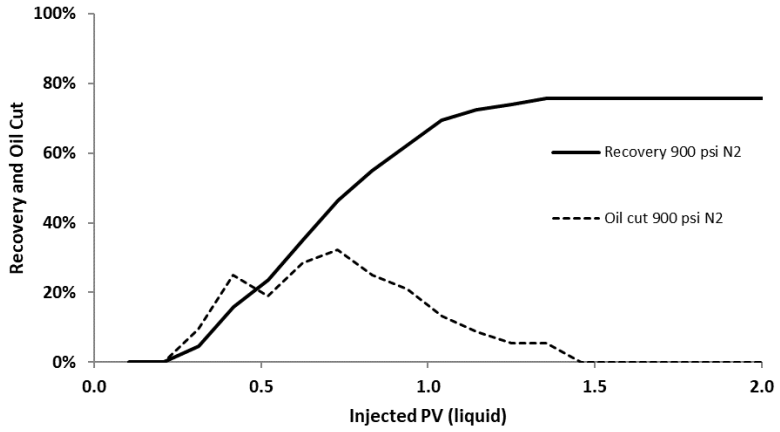

Figure 3.8 Ultimate oil recovery and oil cut from 900 psi nitrogen flood.

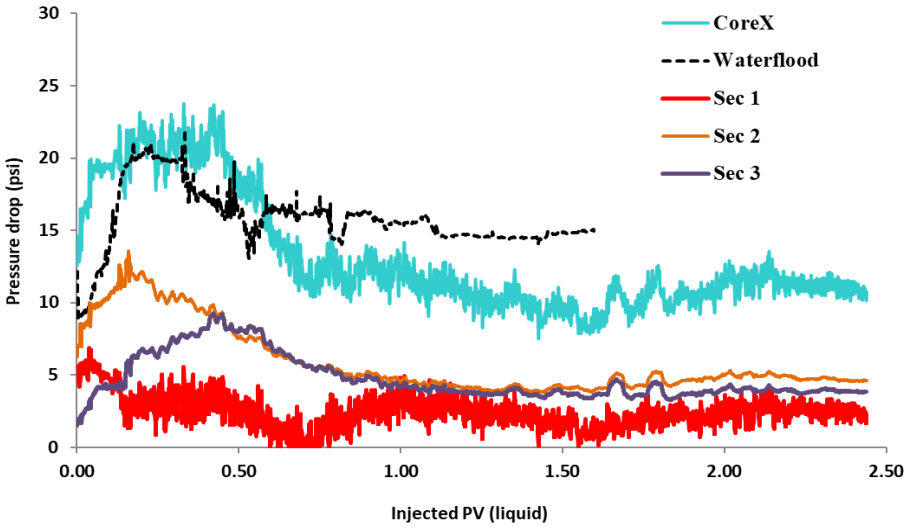

Figure 3.9 Pressure drop data during waterflood and chemical injection of 900 psi nitrogen flood.

The above figures depict the typical oil recovery and pressure drop trends seen in many previously performed nitrogen LTG floods at 50% foam quality (Srivastava and Nguyen 2010; Szlendak et al. 2013). This included first oil breakthrough which is observed around t = 0.3 liquid PV and achieves an oil cut between 25-35% during the peak production of the oil bank. This oil cut remains in this range until the oil bank is fully produced out of the core (t = 1.5 PV). The formation of an oil bank is interpreted not only from the effluent oil cut, but also through observing the pressure drop data. As the oil bank propagates through the core, it generates a higher oil saturation within that section of the core which is occupied by the oil bank. The oil phase has a much lower relative permeability, and thus creates a larger pressure drop within that section. Once the oil bank has propagated through a section of the core, the pressure drop observed in that section of the core is reduced substantially. This trend is seen within the pressure data in Figure 3.9. We see an initial pressure increase in section one, followed by an increase in section two as the newly mobilized oil bank propagates forward. As the oil bank proceeds from section two into section three, the pressure profiles follow as well with a decrease in section two pressure and an increase in section three pressure. Once the pressure in each of these sections decreases, that corresponds to the end of the oil bank being produced out of that section of the core. Looking at the total pressure drop across the core from t = 0.3 to t = 0.5, the greatest pressure drop across the core is observed. This represents the time period with the largest volume of mobile oil, or oil bank, moving within the core. As the total pressure across the core begins to decrease, the mobile oil begins to leave the core out the effluent line. This is seen with the oil recovery plot, where the peak oil cut corresponds to the period where there is the greatest decrease in pressure drop (t = 0.3 PV to t = 1.0 PV). As the oil cut gradually decreases so does the decrease in the pressure gradient across the core. This process continues until t = 1.5 PV, at which point no more oil is being produced and the pressure drop across the core is no longer decreasing. At this point, the pressure across the core is seen to actually begin to increase. This is due to the continuous generation and propagation of foam within the core. As discussed earlier during the foam stability characterization, the presence of oil is detrimental to foam generation. However, at this

point there is far less oil present within the core and the aqueous salinity has deceased towards that of the injected drive salinity which was shown to provide for a better foam generation environment. These trends have been discussed and analyzed before by (Srivastava and Nguyen 2010; Szlendak et al. 2013).

3.4.3.2 Methane Coreflood 900 psi

Following the reference nitrogen coreflood this proof of concept investigation progressed to the modeled associated gases to begin to analyze the effects of hydrocarbon gas on the overall LTG process. The first hydrocarbon oil recovery coreflood performed was with the lean hydrocarbon gas, which was chosen to be modeled by using pure methane. All injection parameters were kept constant between corefloods except for the injected gas. The results for this methane flood are shown in Figure 3.10 and 3.11.

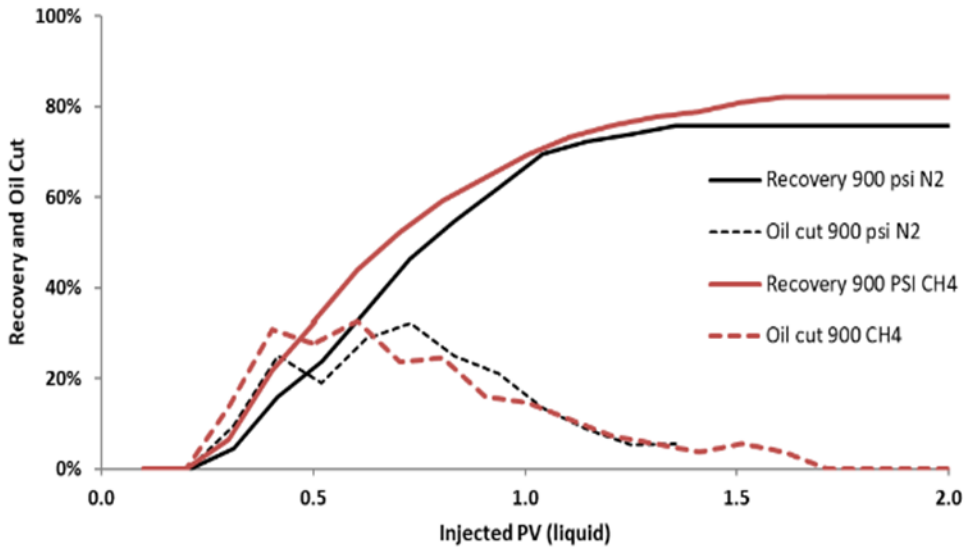

Figure 3.10 Ultimate oil recovery and oil cut results from 900 psi methane flood.

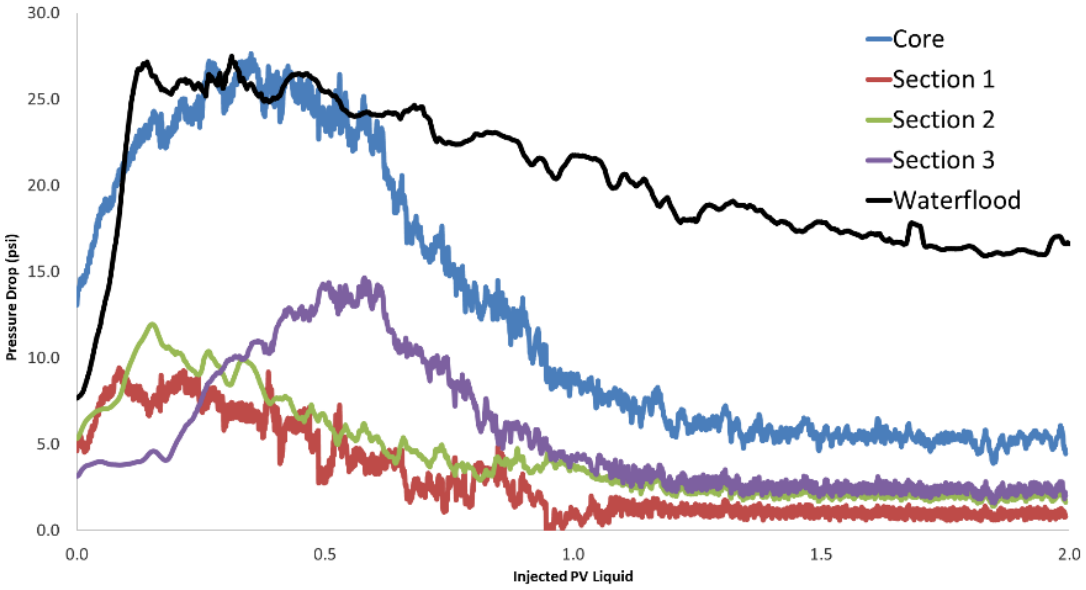

Figure 3.11 Pressure drop data during waterflood and chemical injecting for 900 psi methane flood.

The initial trends seen in both the oil recovery and pressure data appear to be similar to that of the reference nitrogen flood. This was expected from the characterization as there was no substantial shift in the phase behavior optimum salinity and only a slight increase in solubilization ratio between the methane and nitrogen at 900 psi. Initial oil production is seen around the same time of t = 0.3 PV and the oil cut achieves levels between 30-35% from t = 0.4 PV to t = 0.7 PV. This is was nearly identical to the oil bank seen in the nitrogen flood, and expected when comparing to the pressure drop data. The peak pressure drop across the core occurs during this time range, which suggests this is the period with the largest volume of mobile oil moving within the core, which agrees with the observation of the largest oil bank and oil cut at this time. As the pressure begins to drastically decrease at t = 0.7 PV, the end of the oil bank is produced and the oil cut decreases as well. As the oil cut gradually decreases towards zero, so does the decrease in pressure across the core. While the overall trend between the two corefloods appears similar, there are two slight differences that can be explained through the characterization of phase behavior and foam strength. The first of these is that this methane flood has a larger initial oil recovery rate,

resulting in a higher total oil recovery at early time (t = 0.4 – 0.7 PV). After 0.5 PV of injected liquid, the nitrogen flood had produced 24% of the remaining oil after waterflood, while the methane flood produced 32% of the remaining oil by this same time. This increase in early production can be attributed to the slightly higher solubilization ratio seen in the phase behavior. This larger oil cut and recovery is also seen in the pressure data. Both these cores had a very similar permeability and residual oil saturation after waterflood, yet the peak pressure drop for the methane flood reached approximately 25 psi while the nitrogen flood peaked around 22 psi. This is explained by the larger oil bank associated with the higher oil cut seen at this time in the effluent collection. The other difference between the productions of the two floods, was the methane flood had slightly longer production on the tail end. This was likely due to the gradual swelling of the oil that could be achieved as more trapped gas within the core came in contact with the trapped oil. When hydrocarbon gas encounters the trapped oil, it swells the oil increasing its in-situ saturation while also reducing its relative viscosity, allowing this oil to flow more easily. The swelling of the oil likely accounts for the prolonged oil recovery at late time seen with the hydrocarbon gas injection. With the transition to the hydrocarbon gas, the dynamic foam tests had shown that in the presence of Type I microemulsion, a slightly weaker foam could be expected. This too was observed with the pressure drop data during the coreflood at late time once the oil cut had returned to zero. In the nitrogen flood the pressure drop across the core at the end of oil production reached as low as 10 psi, while at the end of oil production for the methane flood the pressure drop across the core reached as low as 5 psi. While the residual oil in the methane flood was slightly lower than that observed with the nitrogen flood, the main disparity in the pressure drop is most likely associated with the characterized decrease in foam strength seen with the hydrocarbon gas in the presence of the Type I microemulsion phase.

3.4.3.3 Methane/Ethane Gas Mixture Coreflood 900 psi

As the objective of this investigation was to understand the effects of using produced gas from the oil field as the injected gas of an LTG flood, the next coreflood was conducted using a hydrocarbon gas on the enriched side of the typical produced gas spectrum. This enriched gas was a hydrocarbon gas composition containing heavier hydrocarbons modeled as C_2+ at a molar ratio of 15% balanced with 85% methane. The results of this flood are presented below in Figure 3.12 and 3.13. During the characterization phase of this investigation very little difference was observed within either the high pressure phase behavior or foam stability characterization between pure methane and the methane/ethane mixture at a pressure of 900 psi, so it was believed that the oil recovery profile would match that of the previous methane flood.

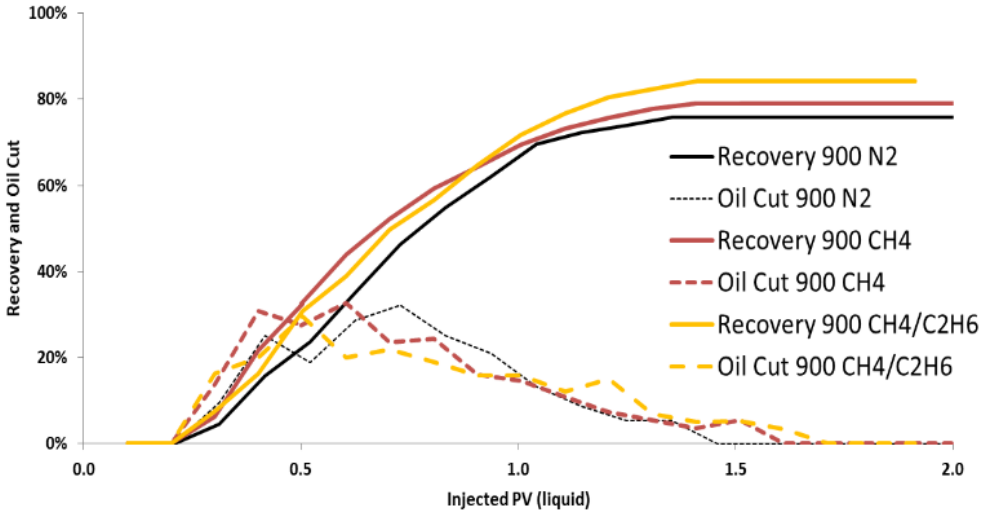

Figure 3.12 Ultimate oil recovery and oil cut results for 900 psi gas mixture.

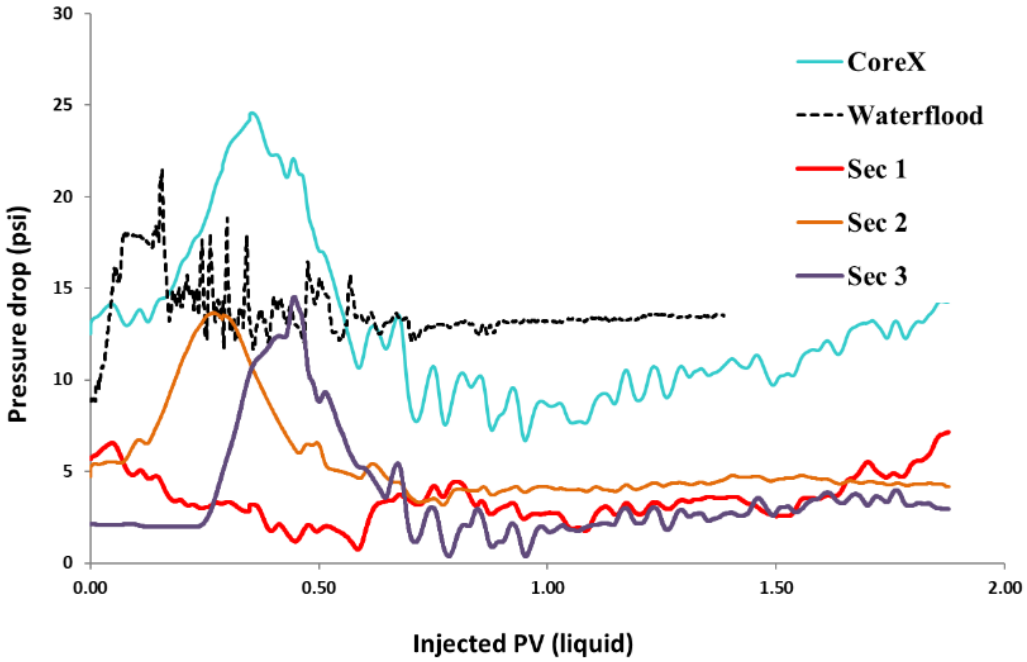

Figure 3.13 Pressure drop data during waterflood and chemical injection of 900 psi methane/ethane gas mixture.

Analyzing the recovery plots, this coreflood produced very similar results to those seen from the methane flood, which was expected based off of what was seen throughout the characterization stages. Oil breakthrough occurred at a similar time of t = 0.3 PV, and displayed very similar oil cut throughout the production of the oil bank. The pressure data displays this same trend of pressure building first in section one (bottom of core), traveling next into section two, and finally entering section three (top of core) right before the pressure drop along the entire core decreases as the oil bank is produced. As stated before, this increase in pressure is from the buildup and mobilization of an oil bank within the core. As oil production is beginning, one simultaneously observes the decrease in the pressure drop. The total oil production mirrored that of the 900 psi methane flood, with the only noticeable difference coming at late time t > 1.0 PV. This slightly prolonged oil production is likely caused by the further increased swelling of the oil from the methane/ethane mixture. From the oil swelling Table 3.1, we see that while methane had a 4.9% increase in volume compared to nitrogen, the mixture gas had an additional 4.3% (9.2% total volume increase) swelling on top of that. This swelling of the oil further increases the in-

situ oil saturation volume and reduces the oil viscosity, allowing it to flow more easily. This swelling of the oil is one of the most promising added benefits observed when the injected gas is switched to a hydrocarbon gas as compared to the more commonly used nitrogen gas. Even when a reservoir pressure is below miscible conditions, some amount of hydrocarbon gas can still disassociate back into the oil phase furthering the oil recovery.

3.4.3.4 Methane Coreflood 1500 psi

For the final oil recovery coreflood, we aimed to investigate the effect of a pressure increase using these hydrocarbon gases in tertiary EOR recovery. The lean hydrocarbon gas composition (pure methane) was chosen as the injected gas for this reservoir with an elevated pressure of 1500 psi. By proceeding with the pure methane gas, the aqueous stabilities would remain the same as there was only a slight shift in the optimum salinity yet would still achieve the increase in solubilization ratio observed with the high pressure phase behavior. With the methane gas we could also compare the effect of the oil swelling to that of the 900 psi mixture gas as they both had a swelling increase near 10% by volume. The results from this coreflood along with all previous corefloods are seen in Figure 3.14 and 3.15.

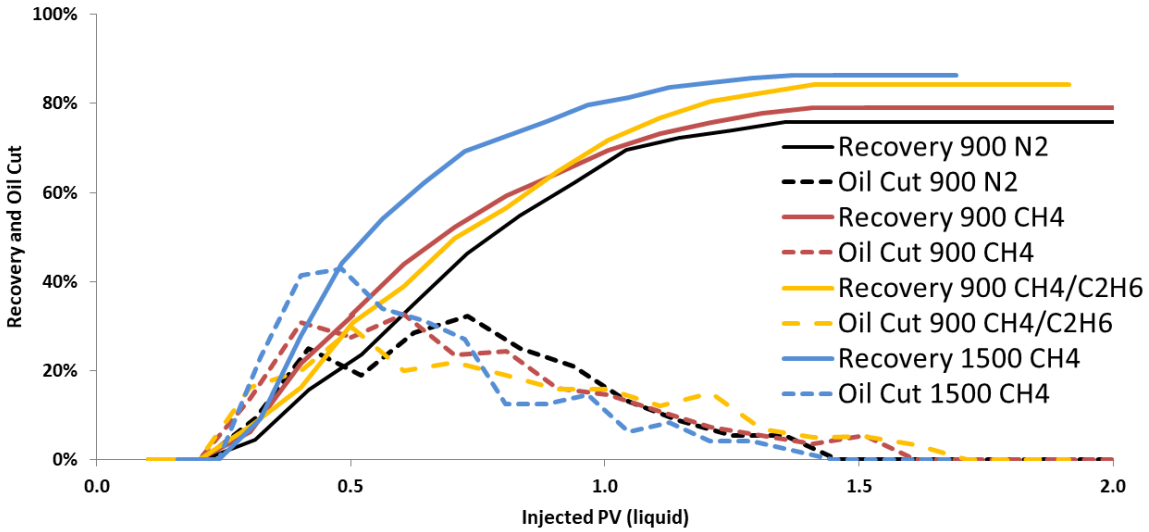

Figure 3.14 Ultimate oil recovery and oil cut results from 1500 psi methane flood.

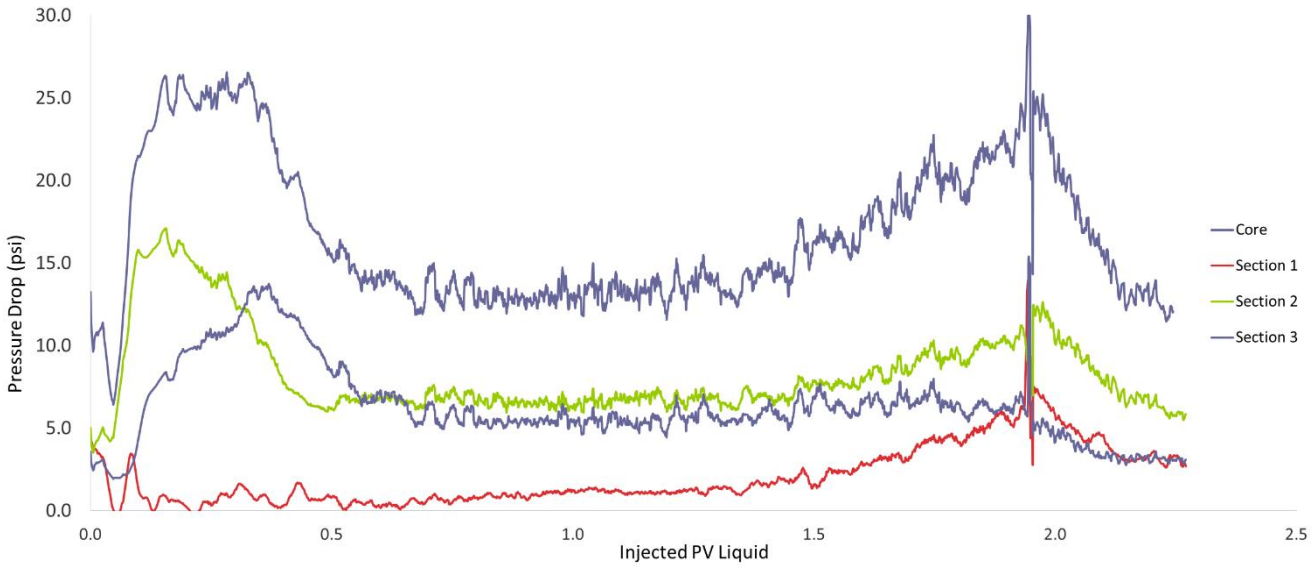

Figure 3.15 Pressure drop data during waterflood and chemical injection of 1500 psi methane flood.

As anticipated from the hydrocarbon characterization, this coreflood not only had the highest ultimate recovery, but also had a much larger initial oil cut leading to a larger initial recovery rate. The oil breakthrough occurred at the same time as the previous floods t = 0.3 PV, but at this time it had a much higher oil cut. This can be attributed to the higher solubilization ratio and thus lower IFT achieved between the oil and aquoues phases at these conditions. From the high pressure phase behavior characterization tests at the elevated pressure, this system achieved a solubilization ratio of 20 for the 1,500 psi methane vs the solubilization ratio of 16 – 17 for the 900 psi systems. An increase in solubilization ratio with the same amount of surfactant results in generating even more of the Type III microemulsion within the core. This reduces the IFT within the system and generates an increased volume of mobile oil seen not only in the effluent analysis but also in the pressure data. While the maximum pressure drop was around 25 psi, which was similar to previous floods at 900 psi, the permeability of this core was higher. This means with a similar pressure drop there must be a larger volume of mobile oil flowing and occupying the pore space, which was what was observed in the effluent collection. At time t = 0.5 PV, where the other floods had only produced 24%, 32%, and 31% of the residual oil to water flood respectively, this 1500 psi coreflood produced 54% of the residual oil.

This early oil recovery becomes increasingly important when viewed on an economic scale, as earlier oil recovery is financially advantageous. The prolonged production associated with oil swelling in the previous hydrocarbon floods does not appear to be as prevelant in this system. This may be attibuted to there being less oil present in the system as larger volumes of oil were produced earlier during the chemical injection. The other aspect of this flood that varied substantailly from the previous floods is the stronger foam that was developed during the drive injection. In the previous floods after achieving 0% oil cut in the effluent we saw pressure drops across the core range from 5-10 psi. However in this flood, the pressure drop remained around 15 psi before it began increasing again after time t = 1.5 PV. At this time, we see the oil cut has gone to zero indicating there is an insignificant amount of mobile oil remaining. This coreflood produced the lowest residual oil saturation, and this lack of oil initiates a more favorable foaming environment. This more favorable environment paired with the higher pressures generated a more stable in-situ foam. This foam strength increased noticably within section 1 and section 2 of the core up until t = 2.0 PV. At this point, it was decided to attempt to destroy the foam within the system to verify that it was in fact foam within the core that was generating the increased pressure drop. This was achieved by replacing the drive solution with an alcohol solution and a dramatic pressure decrease across the core ensued. This occurred because alcohol is known to be extremely detrimental to the foam stability, leading to its destruction. With the injection of this alcohol solution, the pressure drop across the core decreased from 22 psi to near 10 psi within only 0.3 PV of injected alcohol liquid. This proves the existance of trapped gas or foam within the porous media and supports its claim as a suitable mobility control agent, even with the use of a hydrocarbon gas.

3.5 Chapter Summary

Based on the findings discussed throughout this investigation, it can be determined that typical produced hydrocarbon gas compositions ranging from a lean hydrocarbon (pure methane) to that of a more enriched hydrocarbon gas (15% (C_2^+) / 85% methane) can be considered viable gases to be used within a Low Tension Gas flood. In many instances

these hydrocarbon gas compositions were found to have not only performed as well as the more traditionally used nitrogen, but in fact surpassed it in oil recovery rate and ultimate recovery. The transition of injected gas to that of a produced gas had many added benefits, observed in the characterization section. Most notable of these benefits were (i) the increase in solubilization ratio seen between the hydrocarbon gas composition and nitrogen at elevated pressure and (ii) the swelling of the oil and subsequent reduction in viscosity caused by the dissolution of hydrocarbon gas into the oil phase. Utilizing these added benefits of hydrocarbon gas as the co-injected gas phase generates an increase in recovery rate and ultimate recovery seen within laboratory corefloods. With the increase in solubilization ratio, a larger volume of microemulsion can be created, resulting in a larger volume of oil mobilized within the oil bank. This thicker oil bank is the major mechanism providing both the faster recovery rate and also the higher ultimate recovery.

Transitioning to hydrocarbon gas if the opportunity presents itself may be an economically beneficial solution as hydrocarbon gas is produced from many reservoirs where LTG implementation may be of interest. Repurposing this produced gas as the injected gas drastically reduces both the cost of acquiring an injection gas, but also responsibly dealing with the produced gas at the well site as flaring may no longer remain an option. With the observed increase in solubilization ratio during the high pressure phase behavior testing, using a hydrocarbon gas may allow for the amount of surfactant injected to be reduced, and still generate the same oil recovery. This aspect of reducing LTG operation costs by reducing surfactant concentration with the use of hydrocarbon gas injection is a topic of future study and investigation.

CHAPTER 4: Implementation of Produced Gas into Challenging Low Permeability Carbonate Reservoir at High Salinity

4.1 Introduction

The previous chapter of this thesis aimed to establish the general feasibility that hydrocarbon gas could be successfully implemented into the Low Tension Gas design under favorable conditions. However, the main advantage of an LTG flood is its ability to be implemented within diverse and challenging reservoir systems. This current chapter will investigate the performance of produced gas as an alternative to nitrogen gas for mobility control under adverse conditions of low permeability (<100 mD) and high formation brine salinity (180,000 ppm). Additional adverse challenges assumed were that there would be limited access to a low-TDS fresh water supply and a limited supply of produced field gas.

With these added constraints, this study was devised to also attempt to implement a constant salinity injection approach, as a negative salinity gradient design typically used in chemical EOR floods may be difficult to maintain. This required the injection of both the slug and drive to be injected at a high salinity, and the surfactant formulation was designed to achieve this without compromising oil recovery. This constant salinity approach enabled the ability to reinject the produced water, reducing the costs of either processing produced water or acquiring large amounts of additional fresh water. The limited availability of produced gas also generated the need to have the ability to co-inject at reduced gas fractions. This gas fraction was also investigated to determine whether adequate mobility control could still be achieved at a reduced foam quality.

To accomplish the aforementioned goals, the coreflood experiments for this chapter were specifically designed to isolate the parameters mentioned above. An effective surfactant formulation was first developed at atmospheric pressure and reservoir temperature before undergoing high pressure phase behavior experiments similar to those seen in the previous chapter. This surfactant formulation was designed to possess both the ability to generate low interfacial tension between the crude oil and water at the desired conditions, but also generate a foam of adequate strength for an LTG flood. The next characterization performed in this chapter was the impact of gas fraction and whether gas

composition had any effect on the resulting foam stability. Previous studies by Das et al. (2016) had investigated the impact of gas fraction and found that optimum foam quality was a function of the concentration and volume of surfactant being injected. While this previous investigation had used nitrogen as the injected gas, the current study would look at whether similar trends were seen with a hydrocarbon gas as well. The last characterization performed was to analyze how foam strength varied with surfactant concentration as we transitioned from slug to drive. Using the constant salinity approach the only parameter that would change during the coreflood would be the in-situ surfactant concentration in the aqueous phase as the slug concentration was slowly diluted to drive concentration. This transition zone was studied to determine how it would impact foam stability. Following the individual components characterization, a final oil recovery coreflood was performed to determine the synergistic performance of the optimized characterization on oil recovery performance.

4.2 Experimental Materials

4.2.1 Synthetic Brine

The current reservoir under study exhibits produced water with high formation salinity at 180,000 ppm. The composition of the initial formation brine of the reservoir is reported in Table 4.1. This composition is used to prepare synthetic formation brine which can be diluted with deionized water to create the desired salinity for either the microemulsion phase behavior or dynamic foaming and oil recovery coreflooding experiments.

Table 4.1 Synthetic formation brine composition (ppm).

Component	Formation brine
Na^{+}	50,881
Ca^{+2}	14,753
Mg^{+2}	2,153
Cl^{-}	110,604
SO_4^{-2}	300
TDS	180,000

4.2.2 Chemical Surfactant Formulation

Three different types of surfactants were used in this work, including ethoxylated propoxylated carboxylate (Huntsman XOF320C), internal olefin sulfonate (IOS, Shell Enordet O332), and alkyl polyglucoside (APG, Dow Triton CG 650). Before experimentation all aqueous stock solutions were neutralized to pH~7 to improve aqueous stability. The total active surfactant concentration was 1 wt. % in the phase behavior experiments and varied for the foaming and oil recovery experiments.

4.2.3 Crude Oil

The dead crude oil had a viscosity of 1.06 cp and density of 0.84 g/cc at the reservoir temperature of 69 ^{o}C. Before any experimental procedures were performed, this given crude was filtered with 0.8-micron filter paper to remove any suspended solids and fine particles.

4.2.4 Injection Gas Composition

The injected gas compositions used during this chapter are the same as those from the preceding chapter. These gases consisted of pure nitrogen (N_2) for our reference case, a lean produced gas modeled as pure (99+% purity) methane (CH_4), and a more enriched produced gas composition consisting of 85% methane (CH_4) and 15(±0.5) % ethane (C_2H_6) by mole fraction.

4.2.5 Outcrop Cores

The outcrop cores used in this investigation were low permeability Indiana Limestone carbonate cores with the dimensions of 1.5 inches in diameter and 12 inches in length. All cores used during corefloods in this chapter were cut from the same outcrop block in the same orientation. These cores were dry aged at 120º C for at least 10 days before use.

4.3 Experimental Procedure

4.3.1 Microemulsion Phase Behavior

Surfactant formulations were first tested at atmospheric pressure in sealed glass pipets. The successful surfactant formulations were then further tested at high pressure and reservoir temperature in high pressure PVT visual cells in the presence of produced gas. This high pressure phase behavior was conducted with the previously mentioned gases and followed the same procedure as outlined in the previous chapter section 3.3.1.

4.3.2 Impact of Foam Quality and Injection Gas on Foam Strength

The cleaned and vacuumed core was first saturated with brine of 150,000 ppm salinity (prepared by diluting the formation brine in Table 1). This salinity corresponds to the Type III optimum salinity discussed later in this chapter, and the constant salinity which would be used through the course of this foam strength study. After this step, the permeability was calculated to be 30.65 mD. Gas and brine (no surfactant) co-injection was then started at different foam qualities (stepwise change from 80% to 20%). After each step change in the injected foam quality, the system was allowed to attain steady-state pressure drop. The apparent viscosity of the flowing phase was then calculated for each injected foam quality using Darcy's law.

Next, brine was switched to surfactant injection where 150,000 ppm brine with 0.1 wt. % APG (Alkyl polyglucoside – Dow Triton CG 650) was co-injected with gas mixture (85% methane and 15% ethane) at the different foam qualities (decreased stepwise). This foaming formulation was chosen as it is our targeted drive composition during oil recovery

corefloods. This was determined through earlier research at the same experimental conditions conducted by Das et al. 2018, 2020. During each stage of injection the steady state pressure drop was recorded and used to calculate the apparent viscosity of the generated foam. This stepwise process was again repeated with methane co-injected with brine at 150,000 ppm TDS and 0.1 wt. % APG using the same core and described procedure.

All injected fluids were injected from the bottom to the top of the core. Experimental properties and injection parameters are summarized in Table 4.2.

Table 4.2 Properties for dynamic foam strength floods.

Rock type	Limestone
Length	12 in.
Diameter	1.5 in.
Temperature	69 ^{o}C
Back pressure	1000 psi
Total injection velocity	2 ft./day
Injection salinity	150,000 ppm
Injected surfactant concentration	0.1 wt.% APG

4.3.3 Foam Strength in Transition Zone between Slug and Drive

The phase behavior transition between slug and drive was first studied in glass pipets at atmospheric pressure by mixing different ratios of the IFT reducing surfactant slug solution and the foaming drive solution. First aqueous solutions were prepared at 150,000 ppm TDS by mixing the slug and drive formulations at the five different ratios of slug: drive = 0:100, slug: drive = 25:75, slug: drive = 50:50, slug: drive = 75:25, and slug: drive = 100:0. Crude oil was then added to each of these mixtures and the pipets were sealed and allowed to equilibrate at the reservoir temperature of 69 ^{o}C for 1 week. After one week, the pipets showed a variation in microemulsion phase behavior ranging from Type I to Type III due to the difference in the surfactant composition in them even though all of them were conducted at a constant salinity of 150,000 ppm.

This same experimental procedure was scaled up and repeated using larger volumes for the dynamic foam strength test during the transition zone. The aqueous phase of these equilibrated solutions was then extracted and co-injected with the hydrocarbon gas mixture in the coreflood experiments to analyze their foaming characteristics. The initial core was vacuumed for 6 hours to remove any traces of the existing gas phase. Then the core was saturated with 150,000 ppm brine. The experimental parameters followed are the same as those seen in Table 4.2. The aqueous phase extracted from the oil-equilibrated mixture of 100% drive was co-injected with gas mixture (85% methane and 15% ethane) at 30% foam quality. After steady-state pressure drop was achieved, the aqueous phase extracted from the oil-equilibrated mixture of 75% drive-25% slug was co-injected with the gas mixture at the same foam quality. This was continued with the aqueous phase extracted from each of the five previously stated formulation ratios.

4.3.4 Low Tension Gas Oil Displacement Experiments

The knowledge gained through the thorough characterization of the microemulsion and foaming characteristics was employed to assess the efficiency of the developed formulation in displacing oil. The cleaned core was first saturated with 180,000 ppm formation brine, and porosity and permeability were calculated. A special oil saturation procedure was followed in an attempt to increase initial oil saturation and reach close to the connate water saturation in the reservoir under study. Heavy mineral oil was first injected into the core at a low rate, followed by the injection of a light mineral oil, followed by injection of Decalin. Finally, dead crude oil was injected into the core until the effluent oil density matched the previously measured crude oil density. A confirmation phase behavior was run with the final produced oil to ensure that oil characteristics had not been altered and the chosen surfactant formulation still exhibited a satisfactory microemulsion phase behavior. Using this method, a high initial oil saturation (77%) was achieved.

The core was next waterflooded with 125,000 ppm brine until 100% water cut was observed, after which the remaining oil saturation was 27%. This injection salinity was chosen as per the results from the high pressure microemulsion phase-behavior

experiments. The LTG flooding was then started by co-injecting aqueous surfactant slug with the hydrocarbon gas mixture at 30% foam quality. Slug injection was continued for 0.3 liquid PV after which liquid slug injection was replaced by the drive injection containing 0.1wt% APG co-injected with the gas mixture at 30% foam quality. All the injection stages from waterflood to drive were conducted at the same 125,000 ppm salinity, to best follow the constant salinity approach.

Experimental properties and injection parameters are summarized in Table 4.3. Oil cut, oil recovery and pressure drop data were recorded to assess the over success and performance of the coreflood.

Table 4.3 Experimental parameters for oil recovery coreflood

Rock type	Limestone
Length	12 in.
Diameter	1.5 in.
Temperature	69 ^{0}C
Back pressure	1000 psi
Water flood injection rate	2 ft./day
Total slug injection rate	2 ft./day (liquid+gas at 30% foam
Total drive injection rate	2 ft./day (liquid+gas at 30% foam quality)
Gas type	85% methane-15% ethane mixture
Water flood salinity	125,000 ppm
Slug injection salinity	125,000 ppm
Drive salinity	125,000 ppm
Slug composition	Formula 1 in Table 4
Slug surfactant concentration	1 wt.%
Drive composition	0.1 wt.% APG

4.4 Experimental Results and Discussion

4.4.1 Microemulsion Phase Behavior

4.4.1.1 Microemulsion Phase Behavior at Atmospheric Pressure

Two surfactant formulations consisting of an ethoxylated propoxylated carboxylate (Huntsman XOF320C), an internal olefin sulfonate (IOS, Shell Enordet O332), and an

alkyl polyglucoside (APG, Dow Triton CG 650) in two ratios (Table 4.4) were finalized after conducting phase behavior experiments at atmospheric pressure.

Table 4.4 Surfactant formulations of microemulsion phase behavior

Component	Formulation 1 (wt. %)	Formulation 2 (wt. %)
Huntsman XOF320C	0.2	0.27
Shell Enordet O332	0.6	0.53
Dow Triton CG 650	0.2	0.2

For experiments conducted at atmospheric pressure and 69 ^{o}C in glass pipets with the dead crude oil, the optimum Type III salinity for Formulation 1 was 155,000 ppm and for Formulation 2 was 160,000 ppm. The phase behavior results are shown in Figure 4.1 and Figure 4.2.

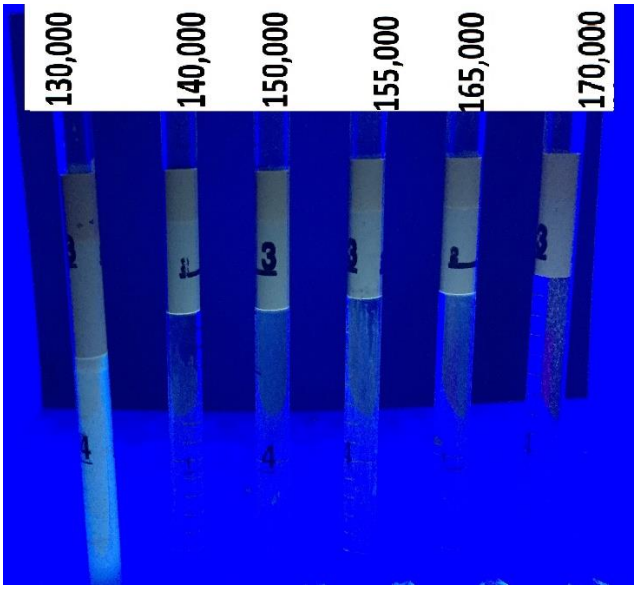

Figure 4.1 Formulation 1 equilibrated microemulsion phase behavior seen under UV light with Type III microemulsion from 140,000 to 165,000 ppm.

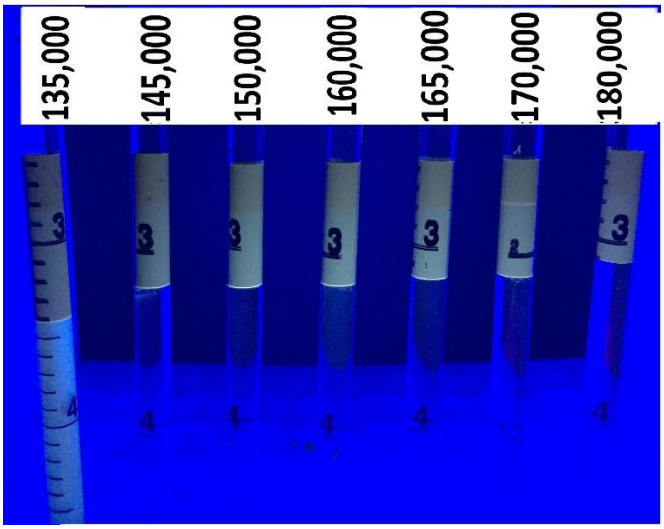

Figure 4.2 Formulation 2 equilibrated microemulsion phase behavior seen under UV light with Type III microemulsion from 145,000 to 170,000 ppm.

4.4.1.2 Microemulsion Phase Behavior at Elevated Pressure

It can be seen from Figures 4.3 and 4.4 that the optimum salinity decreases considerably for both formulation 1 and 2 and the solubilization ratio at this optimum salinity increased in the presence of the gas mixture (85% methane and 15% ethane). An increase in pressure from 1000 psi to 1500 psi was seen to further decrease the optimum salinity, while also improving the solubilization ratios. This is a similar trend with the enriched hydrocarbon gas mixture that is seen in the high pressure microemulsion phase behavior of the previous chapter. While the gas mixture reduced the optimum salinity by roughly 15,000 ppm (Figure 4.3 and 4.4) there was virtually no reduction in optimum salinity for the pure methane gas (Figure 4.5 and 4.6). There was however an increase in solubilization ratio seen amongst both formulations and gas compositions, though it was more extreme for the enriched hydrocarbon gas. The ethane enriched gas mixture had an increase from a solubilization ratio of 10 to 12 and 15 as you increased the pressure to 1000 psi and 1500 psi respectively (Figure 4.3 and Figure 4.4). While the pure methane gas only increased the solubilization ratio to 13 for both of the surfactant formulations at 1500 psi (Figure 4.5 and Figure 4.6).

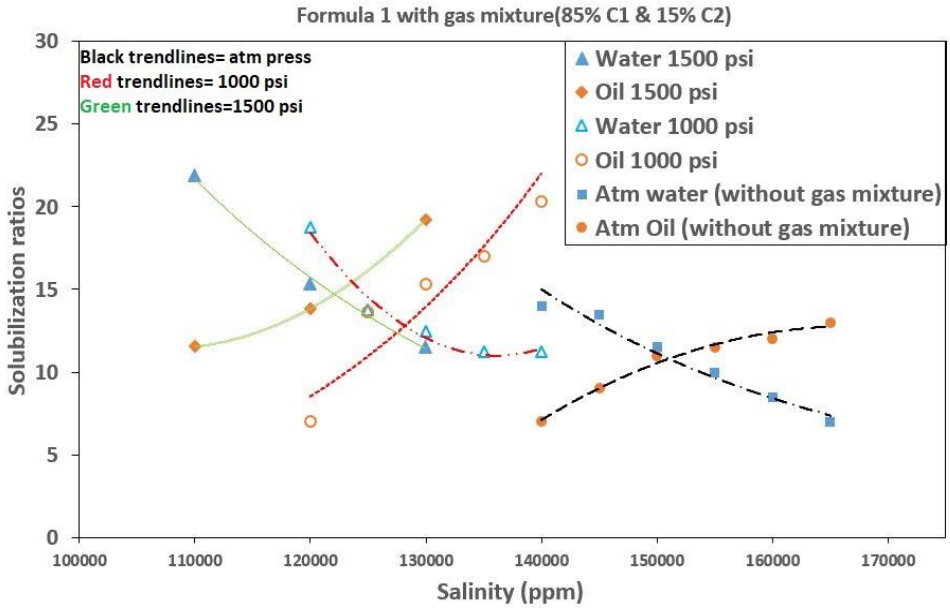

Figure 4.3 High pressure solubilization curves of formula 1 with 85% methane and 15% ethane as the injected gas at different pressures.

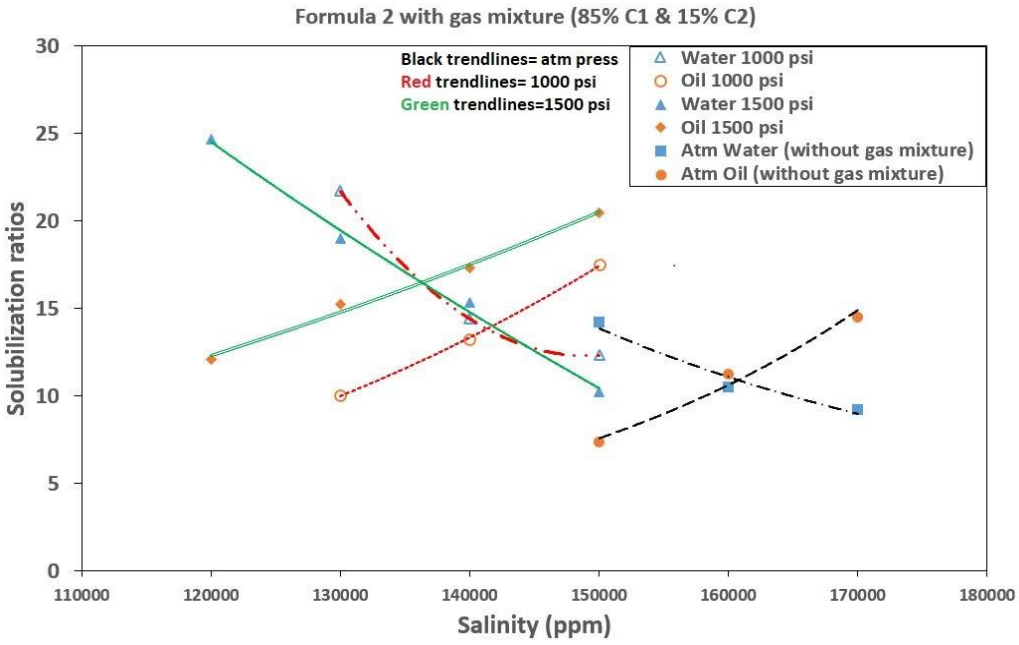

Figure 4.4 High pressure solubilization curves for formulation 2 with 85% methane and 15% ethane as injected gas at different pressures.

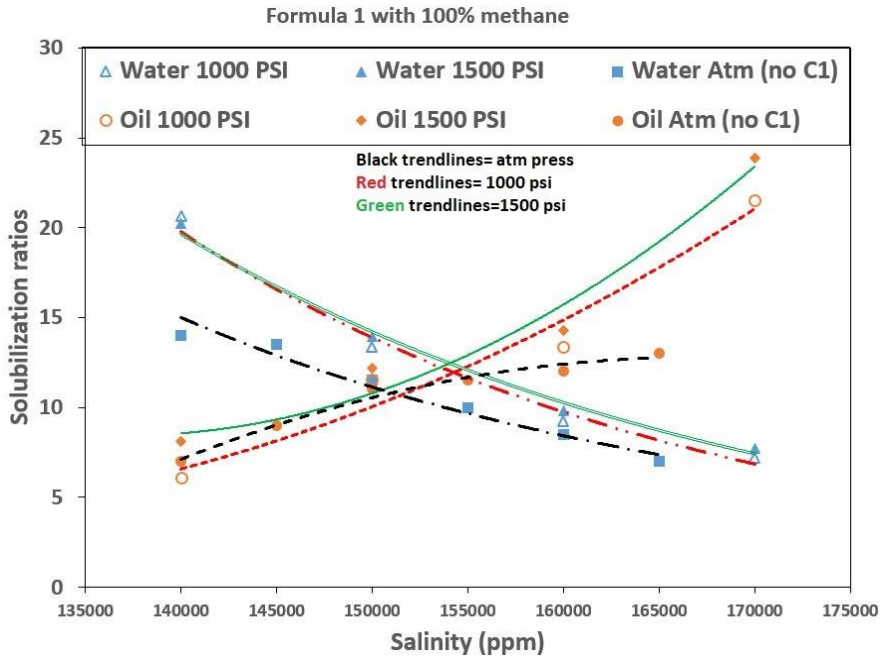

Figure 4.5 High pressure solubilization curves for formulation 1 with 100% methane as injected gas at different pressures.

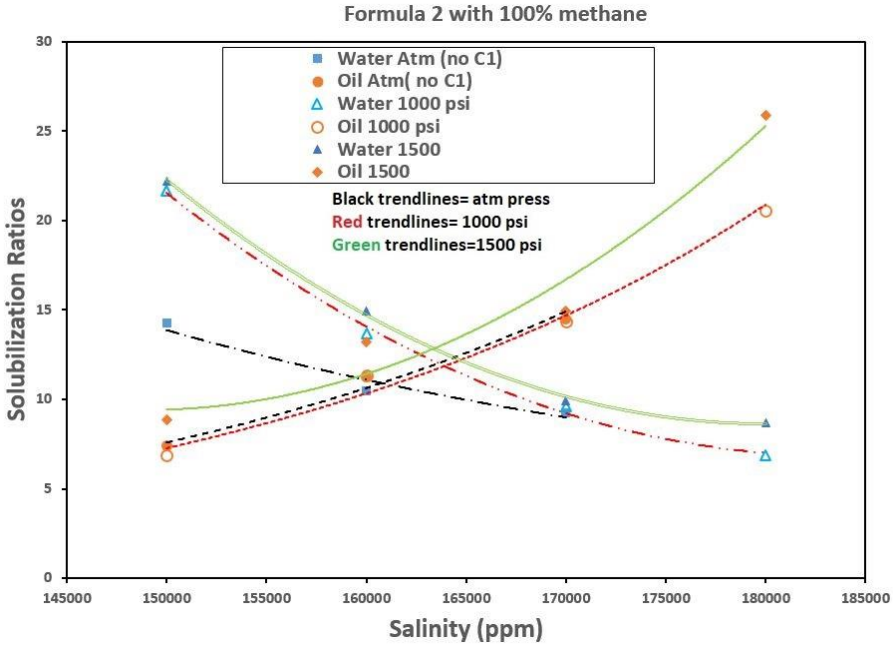

Figure 4.6 High pressure solubilization curves for formulation 2 with 100% methane as injected gas at different pressures.

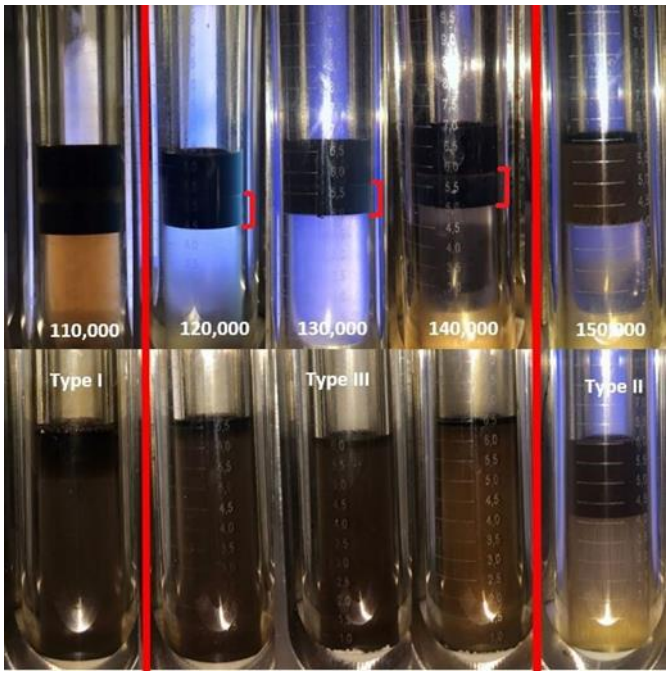

Figure 4.7 High pressure phase behavior tests for formulation 1 seen both before and 10 minutes after shaking in presence of 1000 psi gas mixture (methane/ethane).

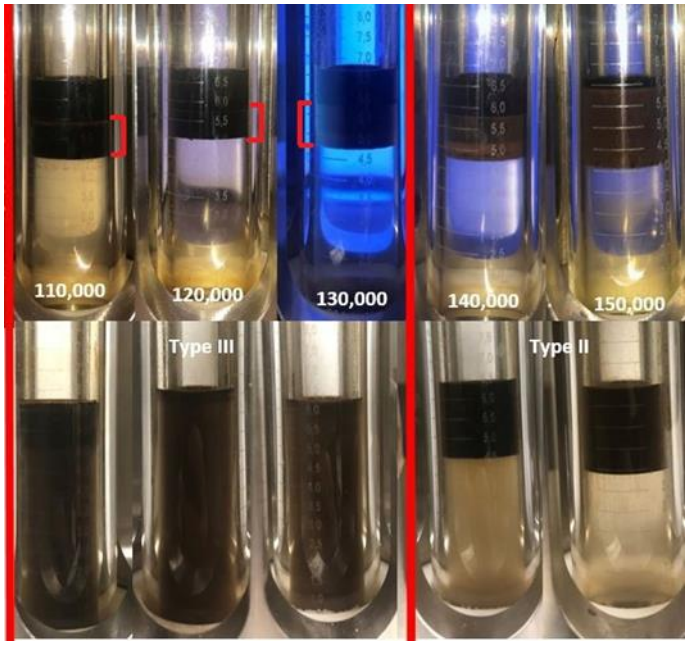

Figure 4.8 High pressure phase behavior tests for formulation 1 seen both before and 10 minutes after shaking in presence of 1500 psi gas mixture (methane/ethane).

From the above experiments, it can be concluded that ethane plays a more prominent role in lowering the Type III optimum salinity and increasing the solubilization

ratios. The next step is to study how the gas composition affects in-situ foaming characteristics. Das et al. (2018, 2020) found that the retention for the IOS surfactant was much larger compared to carboxylates and APG surfactants. Therefore, continuation of experiments involving corefloods Formula 1 was selected because of the higher concentration of IOS to compensate for surfactant retention in the core.

4.4.2 Impact of Gas Type on Optimum Foam Quality

From Figure 4.9, we see the pressure drop is highest for 30% foam quality for both the methane and methane-ethane gas mixture. Because of the limitations of our gas mass flow controller, the minimum foam quality that could be accurately tested was 20%. The type of gas injected does not seem to have any significant effect on the total pressure drop under our experimental conditions. It is important to note that this experiment was conducted in the absence of microemulsion or oil in the system. The interaction of each type of gas will be different with crude oil, mainly in terms of component exchange between the gas and the oil. Therefore foaming properties and resulting foam strength of each gas type might be different after it contacts the microemulsion or remaining crude oil.

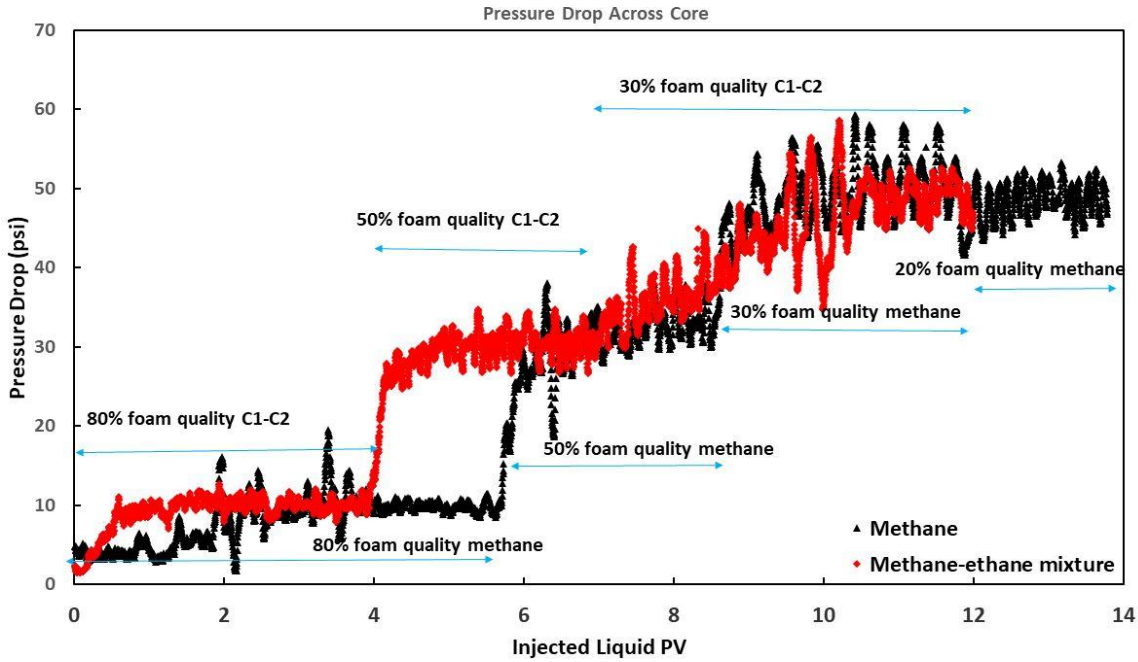

Figure 4.9 Pressure drop across the core for 0.1wt% APG co-injected with different foam qualities of 100% methane and 85% methane / 15% ethane.

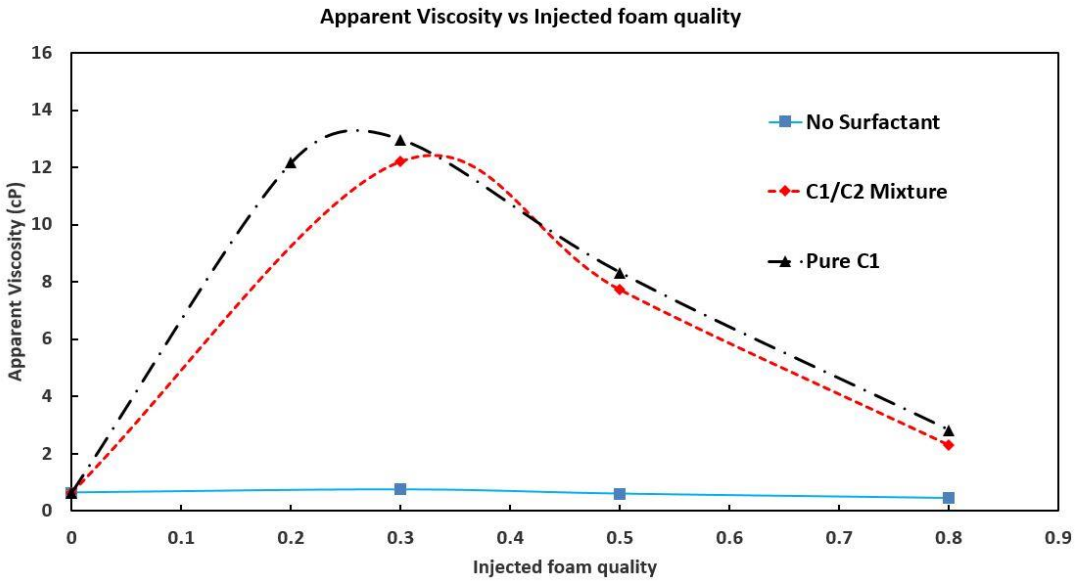

Figure 4.10 Steady-state apparent viscosity generated from the co-injection of 0.1 wt. % APG with different foam qualities of investigated gases.

Figure 4.10 converts these average steady-state pressure drops into apparent viscosity, and shows that it is highest for the 30% foam quality for both gas compositions. The apparent viscosity values are similar for the two gas compositions at a given foam quality. Comparing the values with the no-surfactant case, we can conclude that our formulation could generate significant foam in-situ. Even at 80% foam quality, which produces the weakest foam, the apparent viscosity in the presence of surfactant was much larger than the no-surfactant case.

4.4.3 Foam Strength in Transition Zone between Slug and Drive

Formula 1 Surfactant slug (1 wt. %) was mixed with the drive (APG 0.2 wt. %) at 150,000 ppm in the manner explained prior and allowed to come to equilibrium. This experiment was done to study the transition zone between slug and drive in the reservoir when both are injected at the same optimum Type III salinity using constant-salinity approach. We are interested in the differences in microemulsion phase behavior and foam stability properties between the leading low IFT slug and the trailing foaming drive inside the reservoir, and the transition zone that lies between these extremes.

Results from low pressure phase behavior tests indicate a shift from Type III towards the Type I-III boundary as you approach the mixing ratio of slug: drive= 75:25 (Figure 4.11). This means that in the constant-salinity approach, much of the reservoir remains in Type III or close to the Type III conditions, long after the ultra-low IFT surfactant slug is stopped and the drive injection started. This favorable low IFT Type III behavior can be seen through to the mixing of the slug: drive = 50:50, as after mixing it takes several minutes for separation to occur, indicating a reduced IFT.

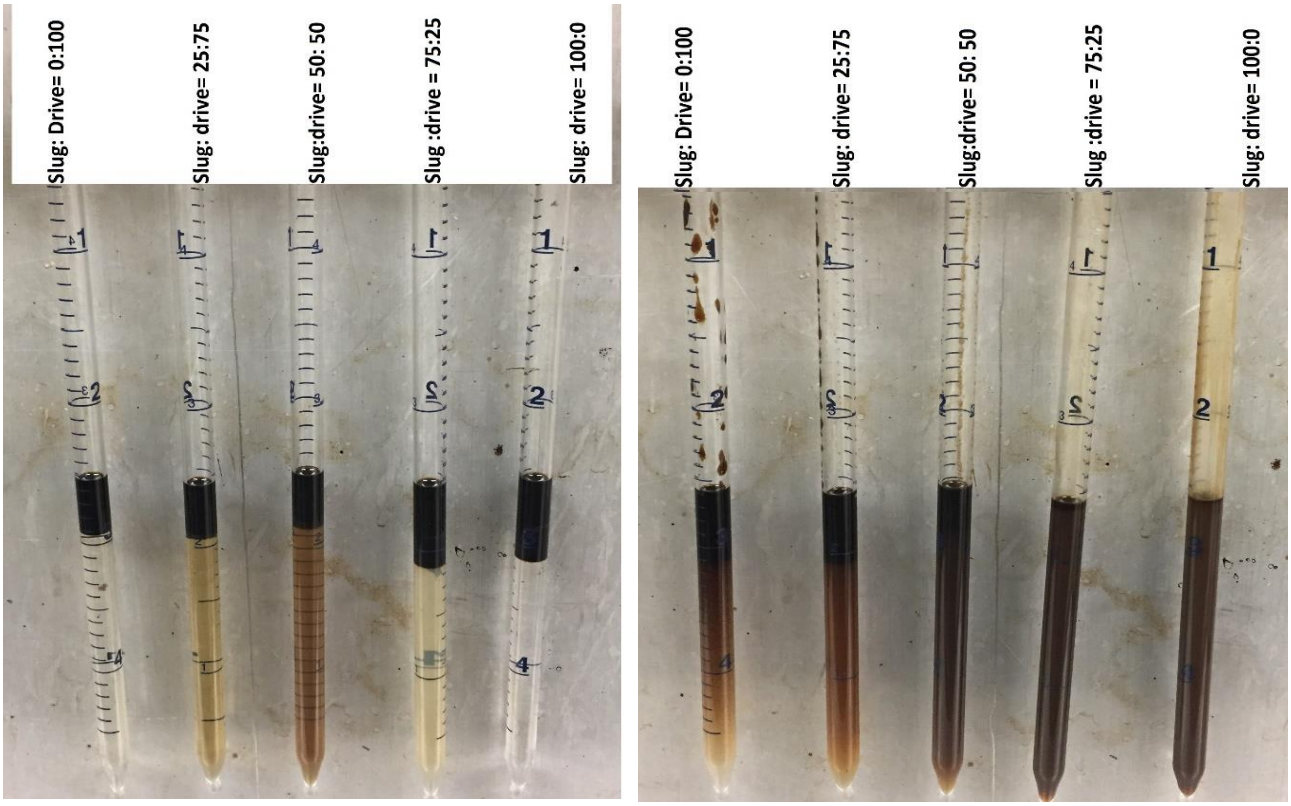

Figure 4.11 Surfactant transition between slug and drive at salinity of 150,000 ppm with formulation 1. Pipets displayed both before and 10 minutes after mixing.

The aqueous phase in each of these five equilibrated microemulsion mixtures was extracted and used for the surface-tension measurements at 25 ^{o}C. Results are presented in Table 4.5. Measurements were done using Pendant drop method.

Table 4.5 Surface-tension measurements at 25ºC (dyne/cm).

0% Slug (Drive solution with oil)	27.59
25% Slug	27.65
50% Slug	27.9
75% Slug	28.24
100 % Slug	32.24
Drive solution (without oil)	27.71
150,000 ppm brine (no oil or surfactant)	76.67

The surface tension (with respect to air) of 150,000 ppm brine without any surfactant or oil is 76.67 dyne/cm. With the addition of the APG surfactant at the drive concentration, the surface tension drops to 27.71 dyne/cm because of the adsorption of surfactant monomers at the water-air interface, which this reduction in surface tension translates to better foam strength compared to brine. This has been established already in the foam-quality scan tests (Figure 4.9 and 4.10). The aqueous phase of the microemulsions in the 0% to 25% slug solutions show surface tension values similar to the drive solution. The aqueous solutions of these mixtures either show no emulsification (0% slug solution) or microemulsion properties similar to that of the Type I range. In these solutions, the oil-swollen micelles exist in equilibrium with the surfactant monomers, which are available to adsorb at the water-air interface reducing surface tension. This means there is sufficient surfactant in the aqueous phase of these four solutions, which leads to surface tension values close to the drive solution without oil. Therefore, the foam strength properties of these equilibrated solutions, 0% and 25% slug, are expected to be similar to that of the drive solution without oil. The 75% and 100% slug solutions are in the Type III range; therefore, it is expected that less surfactant will be available in the excess aqueous phase which has been extracted for these measurements. This is proved by the surface tension for these solutions, which is slightly higher.

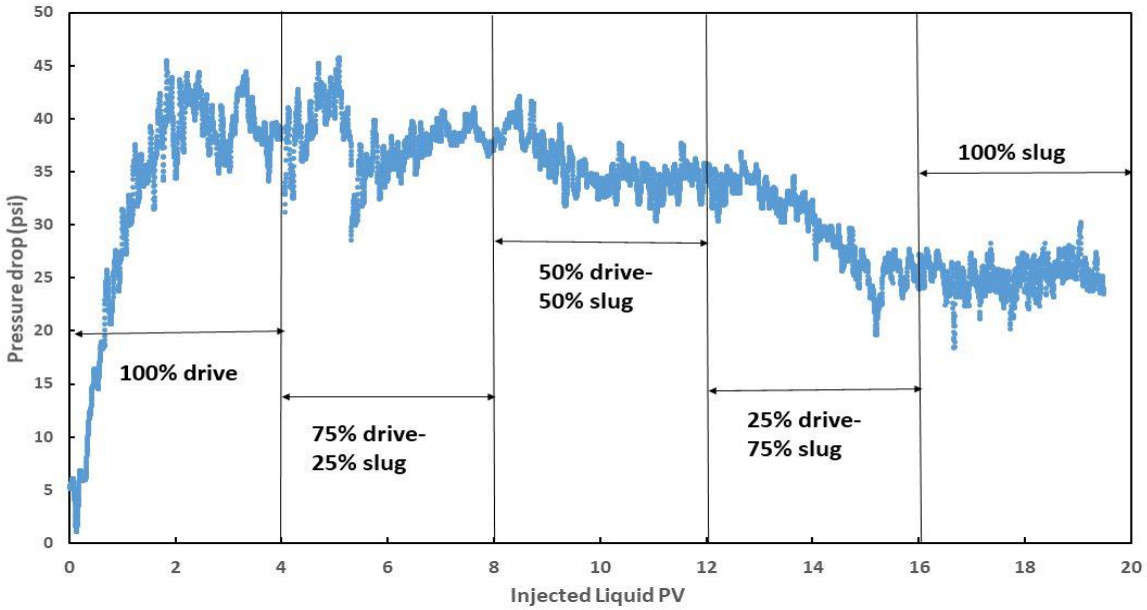

Figure 4.12 Drive to slug transition zone pressure drop across the core during the co-injection of gas and excess aqueous microemulsion phase.

From Figure 4.12, it is observed that the steady-state pressure drop is highest for the 100% drive solution (~40 psi) and lowest for the 100% slug solution (~25 psi). This is what we would have thought through looking at the surface tension measurements of table 4.5. The steady-state apparent viscosity calculated with the 100% oil-equilibrated drive solution is similar to the value (~12 cp) of the drive solution without oil injected at the same foam quality with the gas mixture (Figure 4.10). The pressure drop characteristics seen in Figure 4.12 are in accordance with the predictions of the surface-tension measurements. For the 100% drive and the 75% drive solutions, the steady-state pressure drop values are very similar, since they correspond to Type I microemulsion. The pressure drops slightly in the 50% slug solution, because this is closer to the Type III region. The biggest decrease in the pressure drop is seen during the transition from the 50% slug to the 75% slug solution. The 75% slug and the 100% slug solutions show the lowest pressure drop values, as predicted from the phase behavior and their higher surface-tension values. It is important to note that the steady-state apparent viscosity of the 75% slug and the 100% slug solutions is ~8 cp, which indicates adequate foam strength even in the Type III region.

4.4.4 LTG Oil Displacement Coreflood

Figure 4.13 shows the oil recovery and Figure 4.14 the pressure drop characteristics of the oil displacement coreflood. The permeability of the core for this experiment was 67.85 mD. Residual oil saturation after waterflood (S_{orw}) was 27%. After beginning the tertiary recovery using LTG flooding, ultimate recovery of 68% ROIP was attained after about 2.5 total injected pore volumes of gas and liquid i.e. t_{DT} = 2.5 PV (Figure 4.13). The residual oil saturation at the end of the LTG flood (S_{orLTG}) was 8.8%. The most interesting and attractive observation is the relatively high rate of oil recovery with a recovery of 50% ROIP achieved at t_{DT} = 1.0. The highest oil cut of 30% was observed soon after the end of slug injection. This indicates the breakthrough of a large oil bank with high oil saturation, which was built up quickly because of the combined effect of ultra-low IFT and efficient mobility control provided by the LTG flood. As observed earlier in Figure 4.11, the constant-salinity approach enabled the Type III microemulsion conditions to be extended for a longer duration as the in-situ surfactant concentration approached slug:drive = 50:50. This is in spite of the fact that slug was injected only for 0.3 liquid PV.

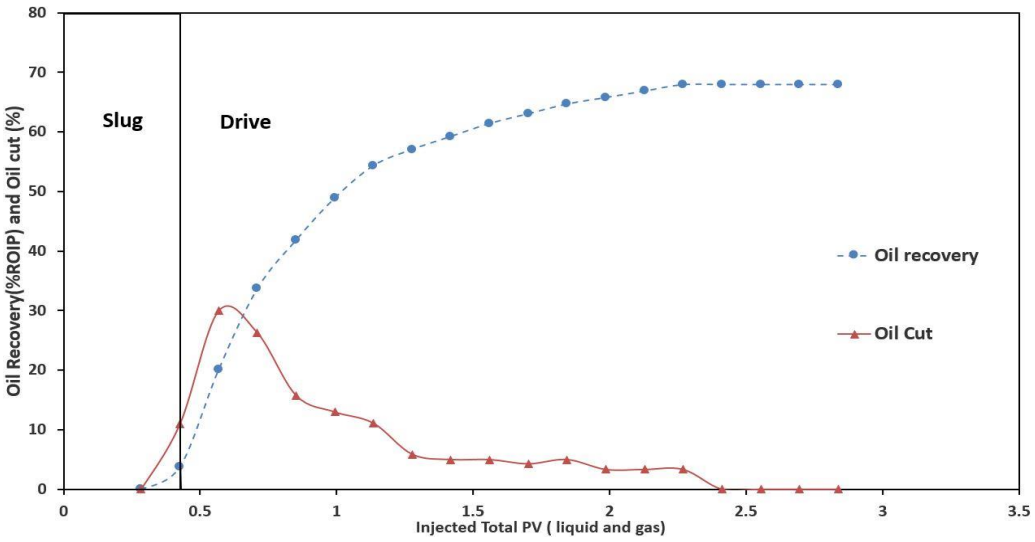

Figure 4.13 Oil recovery and oil rate during LTG injection.

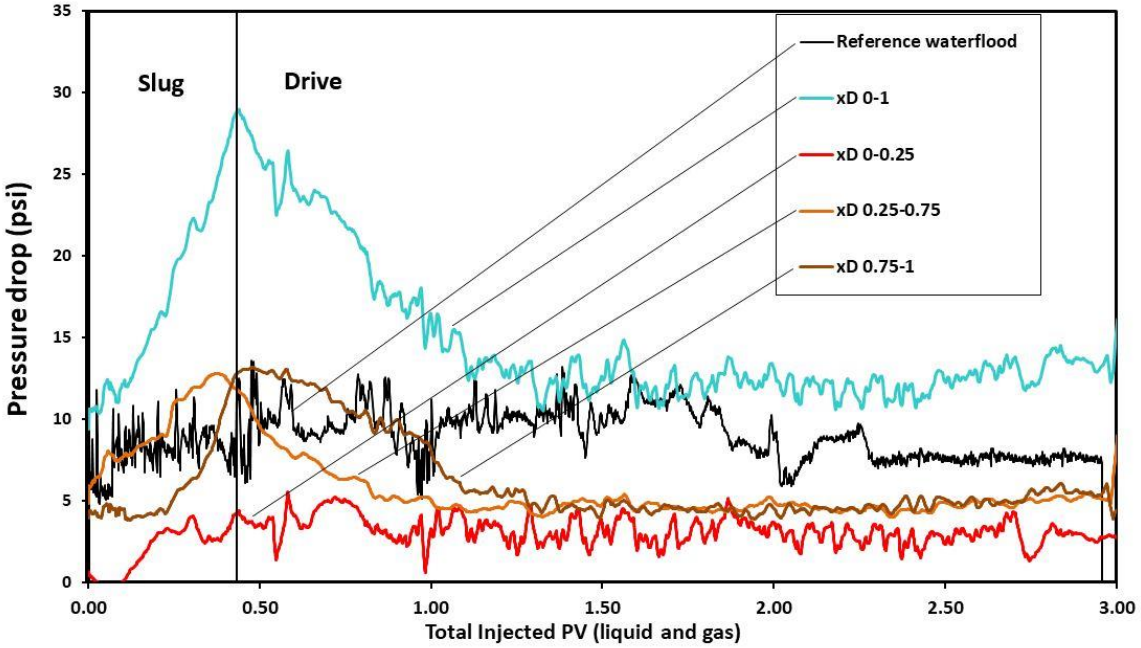

Figure 4.14 Observed pressure drop during LTG injection of oil recovery coreflood.

One key characteristic of the LTG flood is the reduced fluid mobility because of the in-situ generation of foam. The foam lamellae (stabilized by surfactants) cause a reduction in gas mobility by increasing the apparent viscosity of the gas phase. Gas relative permeability is also decreased by the presence of trapped gas, which decreases mobile gas saturation. The increased gas apparent viscosity and the decreased gas relative permeability together, result in reduced gas mobility. In-situ liquid saturation is reduced because of the higher in-situ gas saturation, which results in reduced liquid relative permeability. Thus, the presence of foam reduces the total apparent mobility of both liquid and gas phases (Balan et al. 2011, Balan 2013).

Figure 4.14 shows the sectional and overall pressure drop characteristics of the coreflood. The combined reduced oil-water IFT and the presence of foam causes the residual oil to be mobilized and displaced to form an oil bank. The build-up and movement of the oil bank through the core because of the reduced fluid mobility is concurrent with the increase in the pressure drop in the core. Following the breakthrough of the oil bank, the pressure drop decreases along with the decreased oil cut. The successive sectional

pressure drop trends show an increase and decrease corresponding to the movement of the propagating oil bank through the core. The steady-state pressure drop is achieved by t_{DT}= 2.5 PV, which is about the same time that the ultimate recovery of 68% ROIP is achieved.

In the initial stages of the coreflood (up to t_{DT}= 1.75 PV), the pressure drop during the LTG flooding is higher than that of the reference waterflood. This is because of the effect of the reduced injection fluid mobility as well as the build-up and propagation of the oil bank with high oil saturation. In the later stages (after t_{DT}= 2 PV) , when the core has attained residual oil saturation (S_{orLTG}), the pressure drop for the LTG flood would have been lower than waterflood if there was no foam in the system. This is because S_{orLTG} is much lower (8.8%) than the residual oil saturation after waterflood (S_{orw}= 27%), and so the injected fluids have access to reduced pore volume in case of the waterflood. As such the pressure drop for waterflood would have been higher than LTG flood in the later stages in absence of foam. The higher pressure drop during the LTG flood in the later stages, when there is no more mobile oil in the core, can only be attributed to the generation of foam in the system.

4.5 Chapter Summary

- Low-tension gas (LTG) flooding with produced gas is efficient for tertiary oil recovery in carbonate cores (<100 mD) with high formation brine salinity and high concentration of the divalent cations (Ca^{+2} and Mg^{+2}). Even with a short slug of the ultra-low IFT inducing surfactant, high rate of oil production was sustained by using the constant-salinity approach along with a significant reduction in residual oil saturation.
- In high pressure microemulsion phase behavior experiments, the presence of ethane reduced the Type III optimum salinity significantly as well as increased the solubilization ratios for oil and water. Increase in the pressure further enhanced these effects. The presence of 100% methane did not considerably alter the optimum salinity or solubilization ratios compared to tests with dead oil (no gas).

- With the absence of oil, optimum foam quality (injected foam quality that gave the best in-situ foam strength) was independent of the gas composition. 30% injected foam quality shows the strongest foam corresponding with 0.1 wt.% APG surfactant concentration. Apparent viscosity values for foam generated with both gas compositions (100% methane, and 85% methane +15% ethane) were much higher than merely brine and gas co-injection (no surfactants).
- Foam strength decreases gradually from drive to slug in the transition zone between the slug and drive. However, the apparent viscosity for the foam generated during slug injection was still quite high, indicating good in-situ foam generation and stability in the core even during slug injection (Type III environment).

CHAPTER 5: Conclusions and Future Recommendations

5.1 Thesis Summary

Previous studies have found Low Tension Gas floods to be a promising enhanced oil recovery technique in low permeability reservoirs. These LTG floods are able to generate substantial oil recovery in reservoirs where the use of polymer flooding may not be applicable. In an attempt to reduce the cost of a field scale application of an LTG design, the injection of produced field gas was investigated. Many previous LTG studies utilized nitrogen gas as the mobility control agent, however the transportation or on-site generation of nitrogen may add additional economic constraints. This investigation attempted to analyze the impact of transitioning from nitrogen gas to a typical produced field gas in order to mitigate these expenses. Not only would this eliminate the cost of gas acquisition, but it would also reduce the financial burden associated with processing the produced gas in the field if there is limited market interest. The ability to execute an EOR flood on the field scale at a reduced overall cost is an extremely appealing aspect and the use of produced gas may help.

This investigation first required a thorough characterization as to the effects that an injected hydrocarbon gas could have on the LTG design. An extensive analysis was performed on the impact gas type played on both the microemulsion phase behavior and also the in-situ generated foam strength. A successful phase behavior formulation in the presence of injected field gas is crucial to obtain the ultra-low IFT required to mobilize the trapped oil. With the mobilization of this previously trapped oil a strong foam is also pertinent to provide the desired mobility control to both divert injected surfactant solution into the tighter pores and transport this oil to the production well. There were many different parameters which were considered in the foam stability study. These included the main investigation of gas composition, but it also looked at how this gas composition effect could vary with pressure, the presence of microemulsion, foam quality, and the influence of constant salinity.

The greatest disparity discerned throughout this study was the impact that hydrocarbon gas at an elevated pressure would have on the microemulsion phase behavior.

This discovery also appeared to have a ripple effect into the foam stability as well. It was determined that for both of the crude oil systems in this study that the addition of hydrocarbon gas at an elevated pressure lowered the optimum salinity and increased the solubilization ratio. This increased solubilization ratio is of significant importance because this represents a further reduction in the IFT experienced between the oil and water phases allowing for an increase in oil production or the possible reduction in volume of surfactant injected.

While the addition of hydrocarbon gas benefitted the microemulsion phase behavior, it appeared to be marginally detrimental to the observed foam stability. For the foam stability studies without the presence of oil there did not appear to be a significant difference between gas types, with the hydrocarbon gas producing a similar foam apparent viscosity. However once there was oil present in the microemulsion, gas composition played a much more prominent role. This was likely due to either the increase in oil solubilization seen, or the increase in oil swelling which could decrease the oil phase viscosity allowing it to more easily spread across the film interface.

Combining these effects it was seen that the added benefits of the increased solubilization ratio and oil swelling outweighed the setback of the decrease in foam stability. This was confirmed with the success of the oil recovery corefloods seen both for the sandstone core under moderate reservoir conditions and the limestone core under challenging and adverse conditions. Overall it was concluded that the implementation of produced field gas into the LTG design is not only feasible, but could be advantageous and present different opportunities of reducing the overall cost of an LTG project.

5.2 Future Work and Recommendations

As this investigation was among one of the first in-depth studies into the implementation of produced field gas into the LTG process there are still many areas of potential further study. These important areas of future study include:

- Further study of produced hydrocarbon gas use in more adverse and extreme conditions to determine the feasible limits of its success. This can further unlock potential reservoir candidates for the field scale implementation of the LTG design.
- Further optimization of injection strategy to maximize the full potential of the increase in solubilization ratios and oil swelling.
- Better understanding of the constant salinity approach and how phase behavior and microemulsion can be altered with variations in surfactant formulation and concentration, not just injected aqueous salinity.
- Implementation of produced gas into the LTG design as a form of secondary recovery or tertiary recovery following premature waterflood.

These are just several possible areas of future study to begin to unlock the full potential and economic advantages of implementing produced field gas into the Low Tension Gas design.

References

Austad, T. et al. 1990. Effects of Pressure, Temperature and Salinity on the Multiphase Behavior of the Surfactant/ Methane and n-Decane/NaCl Brine System. *Progr. Colloid Polym. Sci.* 82:296-310.

Austad. T. and Strand, S. 1996. Chemical Flooding of Oil Reservoirs 4. Effects of Temperature and Pressure on the Middle Phase Solubilization Parameters Close to Optimum Flood Conditions. *Colloids and Surfaces A: Physicochemical and Engineering Aspects* 108: 243-252.

Austad, T. et al. 1996. Chemical Flooding of Oil Reservoirs 5. The Multiphase Behavior of Oil/Brine/Surfactant Systems in Relation to Changes in Pressure, Temperature and Oil Composition. *Colloids and Surfaces A: Physicochemical and Engineering Aspects* 108: 253-262.

Balan, H. O., Balhoff, M. T., Nguyen, Q. P. et al. 2011. Network Modeling of Gas Trapping and Mobility in Foam Enhanced Oil Recovery. Energy & Fuels 25 (9): 3974-3987.

Balan, H. O. 2013. Dynamics of Foam Mobility in Porous Media. PhD Dissertation. The University of Texas at Austin, Austin, Texas.

Blaker, T., Aarra, M. G., Skauge, A., Rasmussen, L., Celius, H. K., Martinsen, H. A., & Vassenden, F. 2002. Foam for Gas Mobility Control in the Snorre Field: The FAWAG Project. Society of Petroleum Engineers. doi:10.2118/78824-PA

Bourrel, M., and Schechter, R.S. 1988. Microemulsions and Related Systems. Marcel Dekker Inc, New York, NY.

Bourrel, M., and Schechter, R.S. 2010. Microemulsion and Related Systems: Formulation, Solvency, and Physical Properties. Paris, Editions TECHNIP.

Burruss, R.C., Ryder, R.T., 2014 Composition of Natural Gas and Crude Oil Produced from 14 Wells in the Lower Silurian "Clinton" Sandstone and Medina Group Sandstones, northeastern Ohio and northwestern Pennsylvania. U.S. Geological Survey Professional Paper 1708, 38 p., http://dx.doi.org/10.3133/pp1708G.6. (Chapter G.6 supersedes USGS Open-File Report 03–409.)

Chambers, K.T. and Radke, C.J., Interfacial Phenomena in Petroleum Recovery, Marcel Dekker: New York, 1991.

Cottin, C., Morel, D., Levitt, D. et al. 2012. Alkali Surfactant Gas Injection: Attractive Laboratory Results Under the Harsh Salinity and Temperature Conditions of

Middle East Carbonates. SPE 161727. Presented at the Abu Dhabi International Petroleum Exhibition and Conference, Abu Dhabi, 11-14 November.

Das, A., Nguyen, N., Alkindi, A. et al. 2016. Low Tension Gas Process in High Salinity and Low Permeability Reservoirs. SPE 179839. Presented at the SPE EOR Conference at Oil and Gas West Asia, Muscat, Oman, 21–23 March.

Das, A., Nguyen, N. et al. 2018. Laboratory Study of Injection Strategy for Low-Tension-Gas Flooding in High Salinity, Tight Carbonate Reservoirs. SPE 190348. Presented at the SPE EOR Conference at Oil and Gas West Asia, Muscat, Oman, 26–28 March.

Das, A., Nguyen, N. et al. 2020. Experimental study of injection strategy for Low-Tension-Gas Flooding in low permeability, high salinity carbonate reservoirs. Journal of Petroleum Science and Engineering. Vol 184. January (106564).

Das, A., Nguyen, N., and Nguyen, Q.P. 2020. Low tension gas flooding for secondary oil recovery in low-permeability, high-salinity reservoirs. Fuel. Vol 264. 15 March (116601).

Farajzadeh, R., Vincent-Bonnieu, S., Bourada, N., 2014. Effect of Gas Permeability and Solubility of Foam. *Journal of Soft Matter*, 145-352.

Green, D.W., and Willhite, G.P. 1998. Enhanced Oil Recovery. Richardson, Texas: Society of Petroleum Engineers.

Holt, T., Vassenden, F., & Svorstol, I. 1996. Effects of Pressure on Foam Stability; Implications for Foam Screening. Society of Petroleum Engineers. SPE 35398 paper presented at SPE/DOE symposium on Improved Oil Recovery, Tulsa, Oklahoma, 21-24 April 1996. doi:10.2118/35398-MS

Jang, S. H., Liyanage, P. J., Lu, J., Kim, D. H., Arachchilage, G. W. P. P., Britton, C., … Pope, G. A. 2014. Microemulsion Phase Behavior Measurements Using Live Oils at High Temperature and Pressure. Society of Petroleum Engineers. . Paper SPE-169169-MS. SPE Improved Oil Recovery Symposium. Tulsa, Oklahoma, 12-16 April doi:10.2118/169169-MS

Jong, S., Nguyen, N. M., Nghiem, L. X. et al. 2016. Low Tension Gas Flooding as a Novel EOR Method: An Experimental and Theoretical Investigation. SPE 179559. Presented at SPE IOR Conference, Tulsa, OK, USA, 11–13 April.

Jong, S. 2018. Investigating the Impact of Salinity Gradient Design on Low Tension Gas Flooding Performance. Master's Thesis. The University of Texas at Austin, Austin, Texas.

Kamal, M., Marsden, Jr., S. S. 1973. Displacement of a Micellar Slug Foam in Unconsolidated Porous Media. SPE 4584. Presented at the 48th Annual Fall Meeting of the Society of Petroleum Engineers of AIME, Las Vegas, Nevada, 30 September- 3 October.

Kim, M.W. et al. 1985. Pressure-Induced Critical Phenomena of a Microemulsion System. *Phy. Rev. Lett*. 54(1):46-48.

Kim, M.W. et al. 1988. Pressure Dependence on Multiphase Microemulsions. *J. Phys. Chem*. 92:1226-1230.

Kovscek, A.R. and Radke, C.J., Fundamentals of Foam Transport in Porous Media, University of California, Berkeley, October 1993.

Lu, J. et al. 2013. Recent Technology Developments in Chemical Enhanced Oil Recovery. IPTC 16425. Presented at the International Petroleum Technology Conference, Beijing, China, 26-28 March.

Maini, B.B. and Ma, V., Laboratory evaluation of foaming agents for high temperature applications. Measurements of foam stability at elevated temperatures and pressures, JCPT (November-December 1986) 65-69

Martin, F. D. 1986. Mechanical Degradation of Polyacrylamide Solutions in Core Plugs From Several Carbonate Reservoirs. Society of Petroleum Engineers. Eval. 2, 139-150, SPE-12651 doi:10.2118/12651-PA

Neethling, S.J. Lee, H.T. and Grassia, P., "The growth, drainageand breakdown of foams,"*Colloids and Surfaces A: Physicochemical and Engineering Aspects*, vol. 263, no. 1–3, pp. 184–196, 2005.

Osei-Bonsu, K., Shokri, N., Grassia, P., 2015. Foam Stability in the Presence and Absence of Hydrocarbons: From Bubble to Bulk Scale. Colloids and Surfaces A; Physicochem. Eng. Apsects 481 (2015) 514-526.

Puerto, M.C. and Reed, R.L. 1983. A Three- Parameter Representation of Surfactant/Oil Brine Interaction. *SPE J.* 23(4): 669-682. SPE 10678-PA

Ransohoff, T.C., and Radke, C.J. 1988. Mechanisms of Foam Generation in Glass-Bead Packs. *SPE Reservoir Engineering* **3**(2): 573-585.

Roshanfekr, M., Johns, R. T., Pope, G. A., Britton, L. N., Linnemeyer, H., Britton, C., & Vyssotski, A. 2009. Effect of Pressure, Temperature, and Solution Gas on Oil Recovery from Surfactant Polymer Floods. . SPE-125095-MS. Presented at the SPE Annual Technical Conference and Exhibition, New Orleans, Louisiana, 4-7 OctoberSociety of Petroleum Engineers. doi:10.2118/125095-MS

Sagi, A.R. et al. 2013. Laboratory Studies for Surfactant Flood in Low-Temperature, Low-Salinity Fractured Carbonate Reservoir. SPE-164062-MS. Presented at the SPE International Symposium on Oilfield Chemistry, Woodlands, Texas, 8-10 April.

Saint-Jalmes, A., 2006. "Physical chemistry in foam drainage and coarsening," *Soft Matter*, vol. 2, no. 10, pp. 836–849, 2006.

Schramm, L.L. 1994. Foams: Fundamentals & Applications in the Petroleum Industry. ACS Advances in Chemistry Series 242, American Chemical Society, Washington, DC.

Schramm, L.L. and Wassmuth, F. 1994. Foams: Basic Principles. Article in Foams: Fundamentals and Applications in the Petroleum Industry, Schramm, L. L., Editor, American Chemical Society, Washington, D. C.

Shi, J.-X., & Rossen, W. R. 1998. Improved Surfactant-Alternating-Gas Foam Process to Control Gravity Override. Society of Petroleum Engineers. Paper SPE 39653 paper presented at SPE/DOE Symposium on Improved Oil Recovery, Tulsa, Oklahoma, 19–22 April. doi:10.2118/39653-MS

Sorbie, K. S., & Seright, R. S. 1992. Gel Placement in Heterogeneous Systems With Crossflow. Society of Petroleum Engineers. doi:10.2118/24192-MS

Southwick, J.G. et al. 2012. Effect of Live Crude on Alkaline/Surfactant/Polymer Formulations: Implications for Final Formulation Design. *SPE J*. 17 (2): 352-361. SPE 135357-PA

Srivastava, M., Zhang, J., Nguyen, Q. P. et al. 2009. A Systematic Study of Alkaline-Surfactant-Gas Injection as an EOR Technique. SPE 124752-MS. Presented at the SPE Annual Technical Conference and Exhibition, New Orleans, Louisiana, USA, 4–7 Oct.

Srivastava, M. 2010. Foam Assisted Low Interfacial Tension Enhanced Oil Recovery Process. PhD Dissertation. The University of Texas at Austin, Austin, Texas.

Srivastava, M., and Nguyen, Q. P. 2010. Application of Gas for Mobility Control in Chemical EOR in Problematic Carbonate Reservoirs. SPE 129840-MS. Presented at the SPE Improved Oil Recovery Symposium, Tulsa, Oklahoma, USA, 24–28 April.

Szlendak, S.M. 2012. Laboratory Investigation of Low-Tension-Gas (LTG) Flooding for Tertiary Oil Recovery in Tight Formations. Master's Thesis. The University of Texas at Austin, Austin, Texas.

Szlendak, S. M., Nguyen, N., and Nguyen, Q. P. 2012. Successful Laboratory Investigation of Low-Tension-Gas (LTG) Flooding for Tertiary Oil Recovery in Tight Formations (~10 mD to Gas). SPE 159841-MS. Presented at the SPE Annual Technical Conference and Exhibition, San Antonio, Texas, USA, 8-10 October.

Szlendak, S. M., Nguyen, N., and Nguyen, Q. P. 2013. Laboratory Investigation of Low-Tension-Gas Flooding for Improved Oil Recovery in Tight Formations. SPE J. 18 (5): 851-866.

Szlendak, S. M., Nguyen, N., and Nguyen, Q. P. 2016. Investigation of Localized Displacement Phenomenon for Low–Tension–Gas (LTG) Injection in Tight Formations. *J Petrol Sci Eng* **142**: 36-45.

Zeng, Y., Farajzadeh, R., Eftekhari, A.A., Vincent-Bonnieu, S., Muthuswamy, A., Rossen, W.R., Hirasaki, G.J. and Biswal, S.L., 2016. Role of gas type on foam transport in porous media. Langmuir, 32(25), pp.6239-6245.